Int J Earth Sci (Geol Rundsch) (2007) 96:685–706
DOI 10.1007/s00531-006-0118-2

ORIGINAL PAPER

Structural evolution of the Rides Prerifaines (Morocco): structural and seismic interpretation and analogue modelling experiments

F. Sani · C. Del Ventisette · D. Montanari · A. Bendkik · M. Chenakeb

Received: 17 November 2005 / Accepted: 4 July 2006 / Published online: 6 September 2006

Abstract The Rides Prerifaines (RP) of Morocco constitute the leading edge of the Rif chain. They involve a Triassic–Palaeocene succession deposited on a peneplained Palaeozoic fold belt and accumulated in basins delimited by NE–SW-trending normal fault systems. A significant hiatus separates an overlying Middle Miocene–Upper Miocene foredeep sequence. The reconstruction of the complex structural evolution of the RP during the later compressive phases that affected the Rif chain since Middle Miocene time has been the aim of this paper. We integrated field structural analyses, seismic line interpretation, and analogue modelling in order to evaluate the control exerted by the Late Triassic–Jurassic normal fault systems onto the later compressive tectonics. The maximum compression direction associated with the first compressive phase is roughly NE–SW to ENE–WSW oriented. During this phase the Mesozoic basin fill was scooped-out from the graben and the main décollement level were the Triassic evaporites. Since Pliocene times the maximum compression direction was oriented roughly N–S. During this phase the RP assumed their present structural setting. The earlier normal faults delimiting the Mesozoic graben were reactivated in a strike–slip mode also involving the Palaeozoic basement. The analogue modelling experiments demonstrated that the basement reactivation promoted salt tectonics and favoured fluid circulation.

Keywords Morocco · Rides Prerifaines · Inversion tectonics · Seismic line interpretation · Analogue modelling

F. Sani (✉) · C. Del Ventisette · D. Montanari
Dipartimento di Scienze della Terra,
Università degli Studi di Firenze,
Via G. La Pira 4, 50121 Florence, Italy
e-mail: fsani@geo.unifi.it

F. Sani
C.N.R. Consiglio Nazionale delle Ricerche—Istituto
di Geoscienze e Georisorse, Via Moruzzi 1, 56127 Pisa, Italy

A. Bendkik
Ministère de l'Energie et des Mines,
Direction du Développement Minier,
Rabat-institut, B.P. 6208, Rabat, Morocco

M. Chenakeb
Service Régional de la Géologie de Meknès,
B.P. 39, Meknès, Morocco

Introduction

The Rides Prerifaines (RP; Daguin 1927) or Sudrifaines (Faugeres 1978) constitute the southernmost leading edge of the Rif chain of Morocco and are mainly composed of Mesozoic rocks belonging to the Middle Atlas foreland of this chain (Figs. 1, 2). Their peculiar arcuate shape and the isolated position in the surrounding hilly area, raise the question of their structural evolution in terms of mechanisms and kinematics. The general structure of the RP and their compressive origin has been hypothesized since the 1920s (Gentil 1918; Yovanovitch 1922; Daguin 1927; Bourcart 1932). Later, detailed stratigraphical and structural studies as well as drilling of deep wells for hydrocarbon research provided fundamental contributions to the comprehension of the structure of the RP (Bruderer et al. 1950a, b; Levy and Tilloy 1952; Bruderer and Levy 1954; Taltasse 1953; Tilloy 1955; Burger et al. 1962;

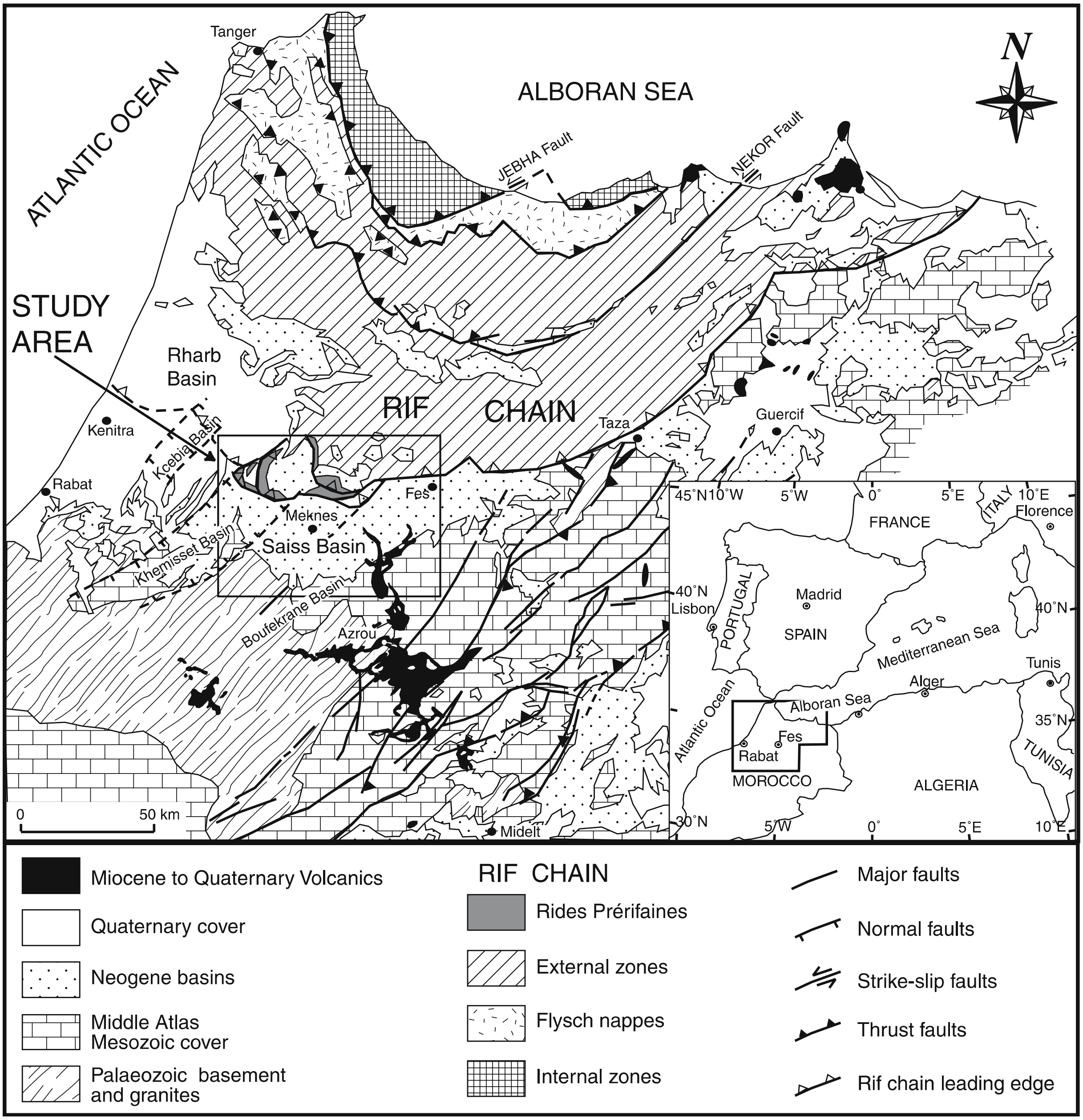

Fig. 1 Geological map of northern Morocco and location of the study area. The subdivision of the structural units follows Michard (1976) and the Carte Géologique du Maroc (1985). The detailed geological map of the study area is shown in Fig. 2. *Inset* shows geographical location of the study area in the frame of Europe and north Africa

Choubert and Faure-Muret 1962; Faugeres 1978, 1981; Aït Brahim and Chotin 1984; Feinberg 1986; Morley 1986; Morel 1988, 1989; Wernli 1988; Boutakiout 1990). More recently, the deep structure of the area has been described by using commercial seismic lines and the available deep wells (Zizi 1996a, b, 2002; Frizon de Lamotte et al. 2004).

These works show that the deep structure consists of a flat peneplained Palaeozoic substratum above which Mesozoic and Tertiary rocks were detached to form a complex of thrust sheets and creating the exposed RP.

One of the major problems arisen from these studies is to understand the role of the previously formed half-graben system during the successive compressive Late Miocene–Early Pleistocene tectonics that affected the area and whether the basement structures were reactivated during the thrusting or not.

Given these uncertainties we adopted a multidisciplinary approach integrating field mapping and structural analyses, seismic line interpretation and analogue modelling. Our data suggest a structural frame in

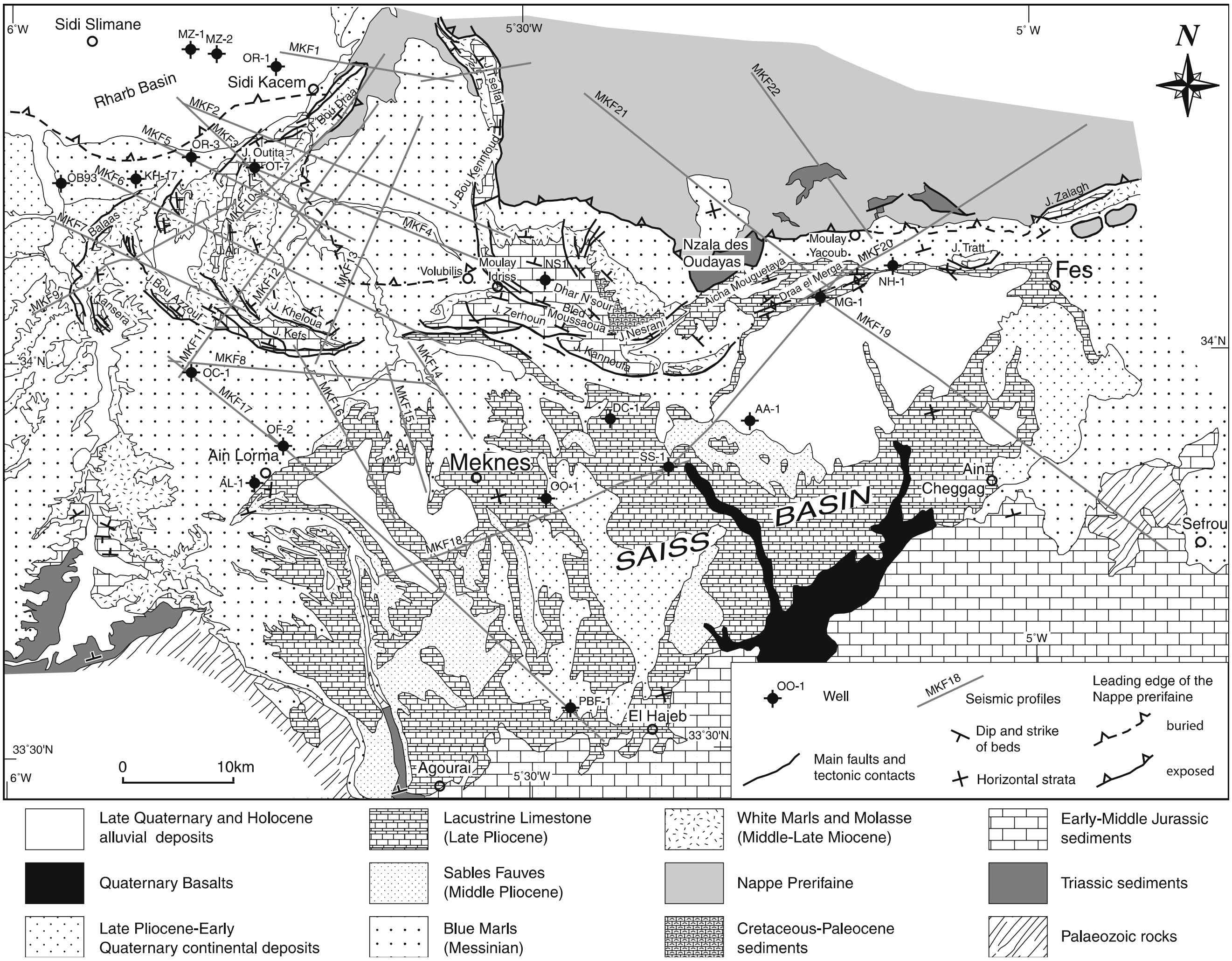

Fig. 2 Geological map of the study area. The grid of seismic profiles used in this paper is indicated, as well as the deep wells whose detailed stratigraphy is reported in Fig. 4

which, under particular conditions, the previous normal fault systems (affecting the Palaeozoic basement) were reactivated with a major strike–slip component, which promoted salt tectonics and favoured fluid circulation.

Geologic setting

The RP involve a Triassic–Palaeocene succession deposited on an almost peneplained Palaeozoic fold belt (Faugeres 1978; Fig. 2). These sequences crop out both at the northern margin of the Middle Atlas chain and within the RP and have been analysed in detail (Faugeres 1978; Boutakiout 1990). This succession has also been penetrated by numerous deep wells so that the Mesozoic stratigraphy is well defined (Fig. 3). Stratigraphic and palaeogeographic studies show that since Triassic times a thick syn-rift succession was deposited within NE–SW-trending basins (Fig. 3). Upper Triassic redbeds deposited in a continental, mainly fluvial environment are overlain by thick (500–1,000 m) evaporites (anhydrites and halite) of Uppermost (?) Triassic–Hettangian deposition age. These evaporites are interbedded with basalts and dolomites. During the Carixian to Bajocian a shallow to deep marine syn-rift sequence contrasts with a much thinner platform succession along the rift flanks. Extension terminated in the Middle-Late Jurassic. A significant hiatus separates the base of a thin Middle-Upper Cretaceous and Paleocene sequence, which is exposed exclusively in the Dahar N'sour area (Fig. 2; Bruderer et al. 1950b; Tilloy 1955; Chenakeb 2004). These sediments may represent a Late Mesozoic–Early Tertiary gulf, whilst the other parts of the present RP emerged (Faugeres 1978, 1981; Zizi 2002).

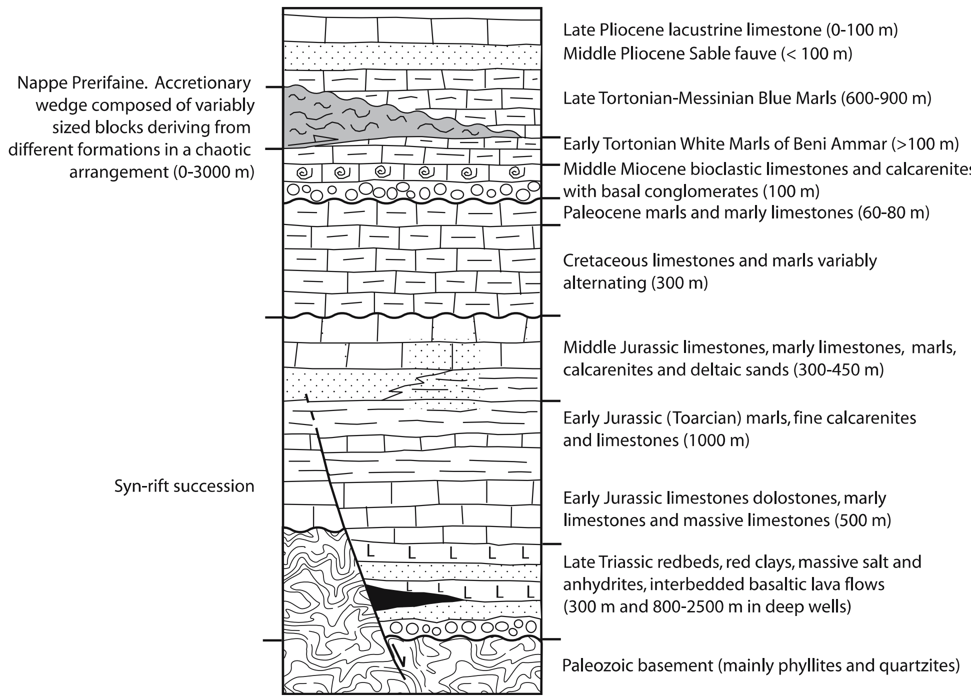

Fig. 3 Composite stratigraphic column of the Mesozoic and Tertiary rocks of the study area (not to scale)

Another important angular unconformity with a major hiatus separates the thin Middle Miocene–Late Pliocene foredeep sequences from the underlying succession (Fig. 3). The foredeep sediments mainly consist of marls (Beni Ammar White Marls and Blue Marls Fm.). Wedged within this marl succession is the accretionary complex of the "Nappe Prerifaine" or the "Prerifaine Complex" [see Bruderer and Levy (1954) for a historical review] that is composed of imbricates, blocks of different lithologies (limestones, sandstones, evaporites among others) chaotically mixed within a clay matrix, gravitational slides and slumps and extensional satellite basins (Flinch 1993, 1996). The emplacement of the Nappe Prerifaine allows to divide the foredeep succession into a pre-nappe and post-nappe sequence, respectively (Faugeres 1978; Wernli 1988 and references therein). Details of this unit are exquisitely shown on seismic profiles across the offshore Rharb area (Flinch 1993, 1996). Deep drillings and seismic profiles in the Rharb as well as the outcrops of this complex close to the RP, allow a precise evaluation of the timing of Nappe Prerifaine emplacement within the foredeep that ranges from the latest Tortonian–Messinian in the study area to Pliocene foreland-ward. Above the Late Tortonian Blue Marls (post-nappe), shallow marine or locally littoral sands (Sable Fauves) are unconformably deposited approximately 100 m thick. These sands are in turn overlain by lacustrine limestones deposited in the great Saïss Basin during Late Pliocene times. Detailed study of this area led to precise evaluation of the extension of the lake (Taltasse 1953). The lacustrine limestone, which is one of the most prominent features of this area, has variable thickness ranging from 10 to 100 m (Taltasse 1953). To the W and NW a marine environment dominated at the same time in the Rharb basin.

The RP have an arcuate geometry in map view (Fig. 2). The major faults strike NE–SW to N–S and mainly NW–SE to E–W. The major ridges coincide with southwest verging thrust faults involving the Neogene foredeep sediments. In particular, the frontal ramps are roughly WNW–ESE oriented, whereas lateral ramps are NE–SW oriented, i.e. parallel to the earlier normal faults. The current morphology is the consequence of the compressive tectonics that affected the area since Late Tortonian time (Faure Muret and Morel 1992). Continuation of the RP below the thin Neogene sediments is seen on seismic profiles and calibrated by wells in the shallow Saïss Basin, which separates the Middle Atlas from the RP (Fig. 2).

The variable orientations of the RP are strictly tied to the trends of the previously formed graben systems inherited since the Late Triassic–Jurassic due to the opening of the central Atlantic Ocean (Faugeres 1978; Boutakiout 1990; Laville and Piqué 1991; Olsen 1997; Laville et al. 2004 and references therein).

Major Mesozoic normal faults strike in a NE–SW direction and crop out at the northern limit of the Middle Atlas namely the Khemisset and Boufrekane basins (Choubert and Faure Muret 1962; Faugeres 1978; Laville et al. 2004; Fig. 2) as well as the Kcebia graben located to the NW, between Kenitra and Sidi Slimane (Figs. 1, 2) and now completely buried below the sediments filling the Rharb basin (Burger et al. 1962; Zouhri et al. 2001).

The structures of the RP based on seismic line interpretation

A grid of commercial seismic profiles that completely covers the study area is available (Fig. 2 for location). The stratigraphy displayed on the lines is also well controlled through numerous deep wells throughout the area (Figs. 4, 5). Previous works by Zizi (1996a, b, 2002), based more or less on the same line grid, were concentrated on the Mesozoic sequence. Our interpretation mainly focuses on the Late Miocene–Quaternary succession and not on the Jurassic sequence. However, our structural interpretation differs from Zizi (1996a, b, 2002) as will be discussed in the following. The lines selected in this paper have been chosen with the aim to elucidate the structural features of the Mesozoic normal fault systems and the associated structures developed during the late compressive tectonics (Figs. 6, 7, 8). Other important points are the structures affecting the RP themselves and the setting of the foredeep sediments within the Meknes-Fes Basin. Moreover, some useful studies have also been carried out about the Nappe Prerifaine emplacement and internal structure.

Some important Late Triassic–Jurassic normal fault systems can be distinguished in the study area (Fig. 5). These fault systems are well imaged on seismic profiles and are evidenced by sudden increase of sediment thickness which is also confirmed by deep drillings (Fig. 4) as already noted by various authors (Levy and Tilloy 1952; Zizi 1996a, b, 2002): (1) The Sidi Fili fault system; (2) the Ain Lorma fault system (3) the Nzala des Oudayas fault system; (4) the Agourai–El Hajeb–Ain Cheggag fault system. All these fault systems played an important role during the later compressive phases that controlled the evolution of the RP.

Sidi Fili fault system

The best known of these systems is the Sidi Fili fault system (Fig. 5), which separates the Rharb basin from the Meknes-Fes (Saïss) basin. It is particularly well imaged from seismic lines and very well controlled by

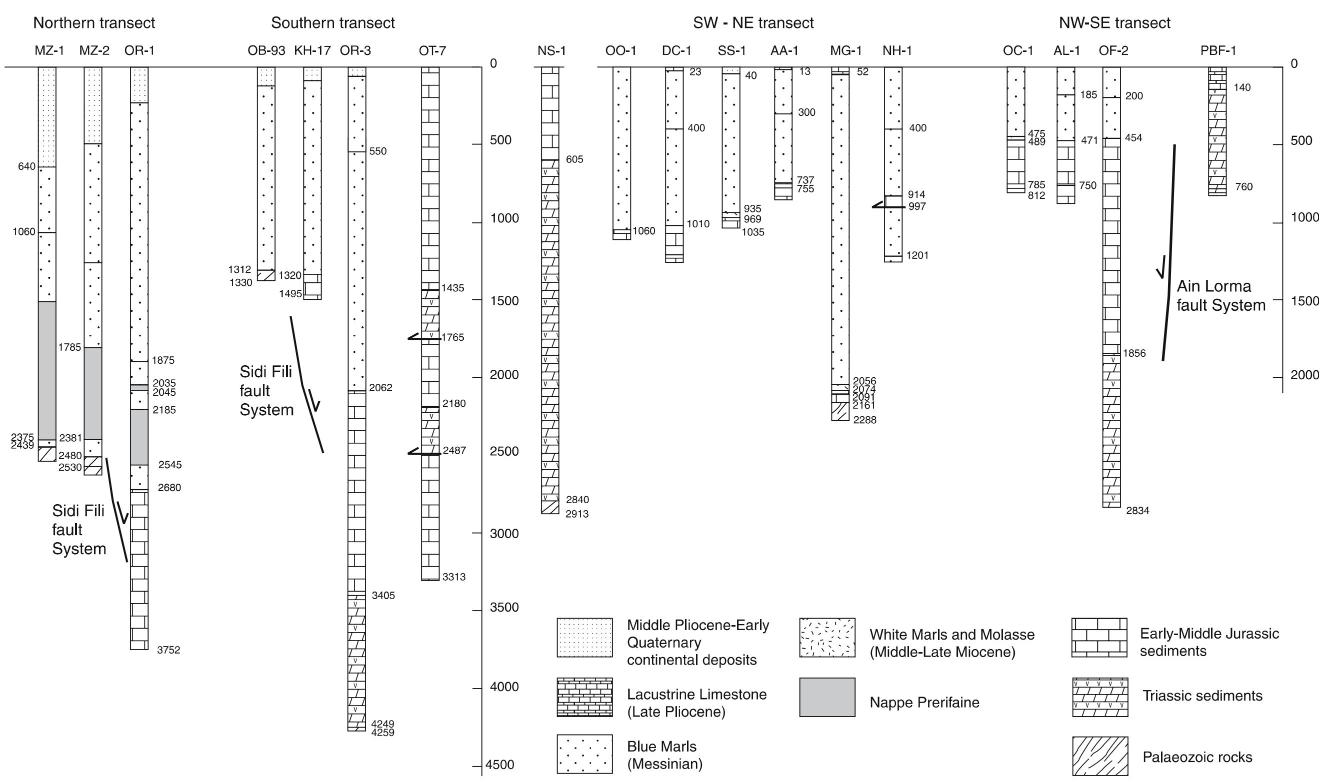

Fig. 4 Logs of wells utilized in this paper. For location see Figs. 2 and 5

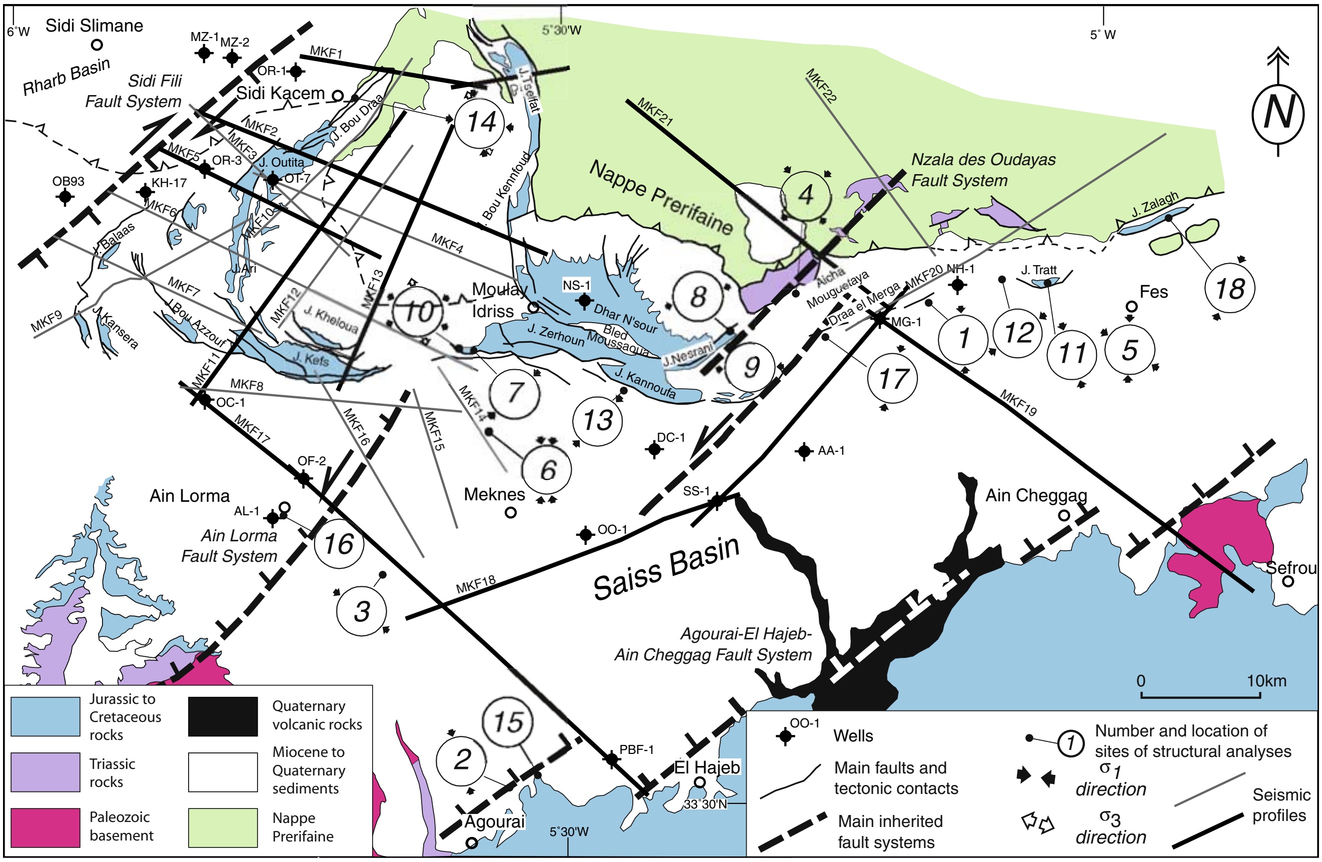

Fig. 5 Structural sketch map of the study area. Seismic profiles used in this paper are shown. *Bold lines* indicate seismic profiles whose line drawing is reproduced in Figs. 6, 7, and 8. Major Mesozoic normal fault systems are indicated as inferred by seismic profiles analysis, well logs and field evidence. Location of sites of structural analysis (plots in Fig. 12) is also indicated

drillings, considering that the major oil fields of the area are located along this system (Levy and Tilloy 1952; Costagliola et al. 1997; Jabour et al. 2000; Zizi 2002). Figure 6 shows interpretations of lines MKF2 and MKF5, which cut across the Sidi Fili fault system and show a northwestern Palaeozoic shoulder on which thin Mesozoic sediments were deposited in contrast to the thick infilling of the adjacent graben. The major fault cuts through the Hercynian basement at depth (Figs. 4, 6). Northward, this abrupt increase of Mesozoic thickness is well documented by MZ-1 and MZ-2 wells in contrast to OR-1 well (Fig. 4). The Sidi Fili fault system delimits the Khemisset basin to the northwest (Figs. 1, 2). This basin crops out along the northernmost border of the Middle Atlas. Roughly parallel to this fault trend is the alignment of Jebel Bou Draa–Jebel Outita–Jebel Balaas that constitutes a lateral ramp of the detached thrust system. In the seismic lines the complex setting corresponding to this structure with at least three tectonic repetitions (well OT7, Fig. 4) and the increased thickness of Triassic evaporites is evident (Figs. 6, 7, 8).

Ain Lorma fault system

This system constitutes the southeastern shoulder of the exposed Khemisset basin, and it defines the NE limit between the external and internal RP (Suter 1980a, b). The Ain Lorma Fault System is very well imaged along the MKF16 and MKF17 seismic lines crossing the Meknes-Fes basin in a NW–SE direction (Figs. 2, 8). Both the seismic lines and the well OF-2 show an increased thickness of the Mesozoic sequence toward the normal fault. With the master fault are also associated less pronounced antithetic faults, all involving the Palaeozoic substratum. The Ain Lorma fault system does not reach the surface but affects the basal portion of Neogene foredeep sediments. The northeastern extension of this fault system is uncertain; only section MKF6 may reach the northeastern part of this fault system but the overall structure is not clear. It shows some up-dip convergence of Jurassic reflectors connected with a salt pillow at depth (Zizi 1996a, 2002) and a complex structure that probably is due to the westernmost propagation of the Jebel Zerhoun thrust

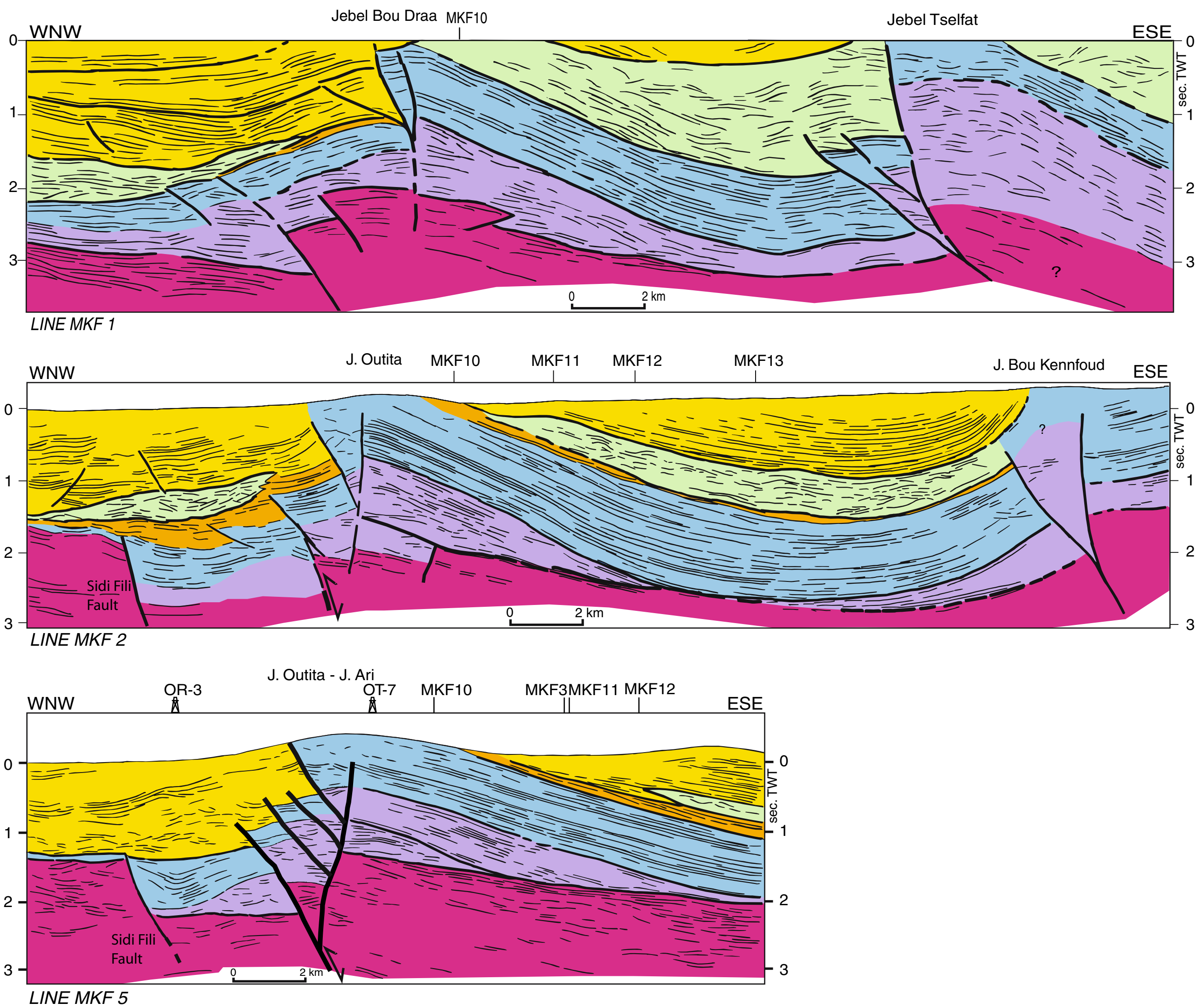

Fig. 6 Line drawings of structural interpretation of lines MKF1, MKF2, and MKF5. For location of lines see Figs. 2 and 5. The *colours* indicate different units as follows: *light red* undefined Palaeozoic basement units; *violet* Triassic units and evaporites; *light blue* undefined Jurassic units; *light brown* Early-Middle Miocene foredeep units below the NP; *light green* Nappe Prerifaine complex; *yellow* Late Miocene foredeep and recent deposits of Saïss basin

fault. More to the north (Fig. 2) the abrupt southern termination of the Jebel Kennfoud Jurassic outcrops (Bendkik 2004), the eastern termination of the Jebel Kefs ridge, the arcuate shape and the offset between Jebel Zerhoun and Jebel Kefs ridges may indicate the presence of a NE–SW striking buried fault.

Nzala des Oudayas fault system

This third fault system delimits the internal RP to the SE (Jebel Kannoufa, Jebel Nesrani) and is evidenced, in map view, by the alignment of the Triassic halite and anhydrite outcrops of Nzala des Oudayas (Fig. 2; Zizi 1996a, 2002) and by the eastern termination of the Jebel Kannoufa and Jebel Nesrani ridges; the latter shows a marked NE–SW trend, i.e. parallel to the Nzala des Oudayas outcrop trend and probably coincident with a lateral ramp of the major Jebel Zerhoun thrust front (Fig. 5). The presence of a deep fault is also revealed and confirmed by a seismic line running in a NW–SE direction through the Triassic outcrop (Line MKF 21, Fig. 7). The seismic line shows Triassic rocks, mainly composed, at the surface, of anhydrites, massive salt as well as clays with embedded basalts, which came up from depth as already supposed by Zizi (1996a, 2002). In our interpretation the uprising of Triassic rocks may be due to the reactivation of an earlier normal fault affecting the basement, whose

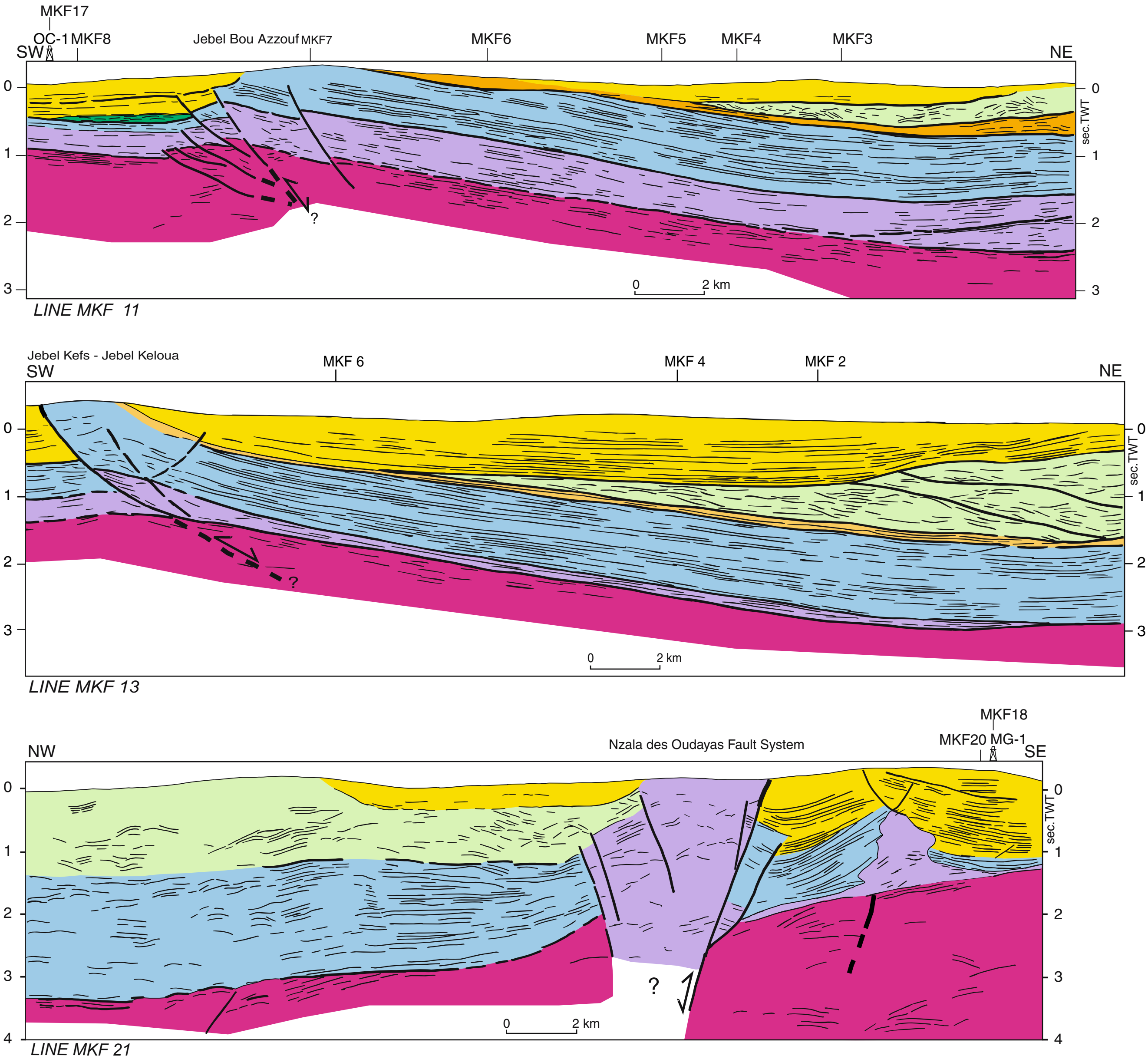

Fig. 7 Line drawings of structural interpretation of lines MKF11, MKF13, and MKF21. For location of lines see Figs. 2 and 5. For colour legend see Fig. 6

presence is revealed by the different thickness of Jurassic sediments on both sides of the fault (line MKF21, Fig. 7). The reactivation of the fault may have promoted the growth of a diapiric structure during the Neogene and Quaternary compressive phases (Del Ventisette et al. 2005) in a similar way as described by Vially et al. (1994). The presence of a basaltic neck whose setting is not comparable with other basalts occurring in the same area which are clearly embedded within the Triassic red clays should also be noted. This neck soars above the surrounding hilly landscape and can be clearly seen from a long distance. Unfortunately, the alteration of basalt did not allow a radiometric age determination but in our opinion its emplacement is connected with the strike–slip fault reactivation, which may have caused its recent uprising from depth. Along the seismic section MKF21 (Figs. 5, 7) another diapiric structure is also imaged which is related to the reactivation of a minor normal fault affecting the basement, roughly parallel to the major one (Del Ventisette et al. 2005). An indirect validation of this hypothesis is the deformation of the Neogene and Quaternary sediments at the surface, such as the en-echelon arrangement of NE–SW-trending anticlines

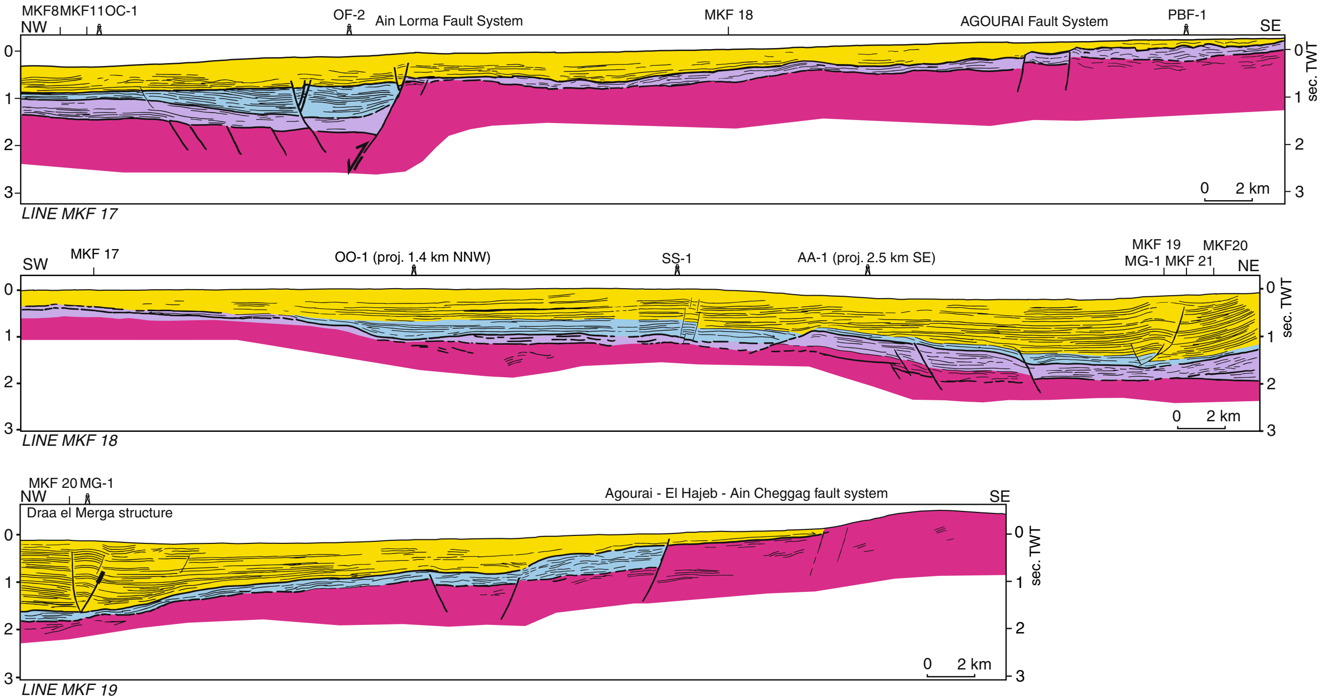

Fig. 8 Line drawings of structural interpretation of lines MKF17, MKF18, and MKF19. For location of lines see Figs. 2 and 5. For colour legend see Fig. 6

involving the Late Pliocene Lacustrine Limestones (Figs. 2, 5). One of these structures has been explored by the MG-1 well (Figs. 4, 9). Moreover, the well-known Aicha Mouguetaya structure (Taltasse 1953), also affecting the Lacustrine Limestone shows a strong deviation of strike in this area, suggesting recent activity along the transversal Nzala des Oudayas structure (Figs. 2, 5).

Agourai–El Hajeb–Ain Cheggag fault system

This fault system constitutes the northwestern limit between the Meknes-Fes basin and the Middle Atlas chain (Fig. 2). This system does not seem to be an inherited Mesozoic normal fault system. Two seismic sections cut across this system and the faults are well imaged on seismic lines (Lines MKF17 and MKF19, Fig. 8). From the comparison of line MKF17 with MKF19, a Jurassic activity of this system can be inferred, considering the thickness of sediments on section MKF19, although the lack of Triassic sediments in the MG-1 is not clear (Fig. 4). In contrast, section MKF17 shows the lacking of Jurassic sediments and, at well PBF-1, the Neogene and Quaternary deposits rest directly on Triassic rocks. In map view, these faults show a right stepping en-echelon arrangement (Fig. 5), suggesting a left-lateral component along the Middle Atlas border, as suggested by many authors (Jacobshagen et al. 1988; Morel et al. 1993; Bernini et al. 2000; Frizon de Lamotte et al. 2004). In the field the segment close to Ain Cheggag shows very good exposures (Figs. 2, 10).

The Nappe Prerifaine and the Meknes-Fes basin

As already noted by different authors (Levy and Tilloy 1952; Flinch 1993, 1996; Zizi 2002 and references therein), the Nappe Prerifaine is deeply involved in thrusting as well as in the more recent deformation, and the present setting of the RP follows the emplacement of the NP (Figs. 6, 7). The buried front of the NP has been traced using the available seismic lines in the Volubilis Plain (Fig. 2), whereas in the Rharb basin its trace has been compiled from different works (Bruderer and Levy 1954; Burger et al. 1962; Flinch 1993, 1996 and references therein). The seismic image of the NP is quite typical and reflects its lithological features. It is composed of disrupted portions of different sequences variable in size, age and composition, similar to other accretionary wedges (e.g. Ligurian Units accretionary wedge of the Northern Apennines: Vannucchi and Bettelli 2002; Bettelli and Vannucchi 2003 and references therein). As a consequence, on seismic lines it is imaged as discontinuous and variably oriented reflectors (Figs. 6, 7). Within the Nappe Prerifaine thrust faults splaying from the base to the

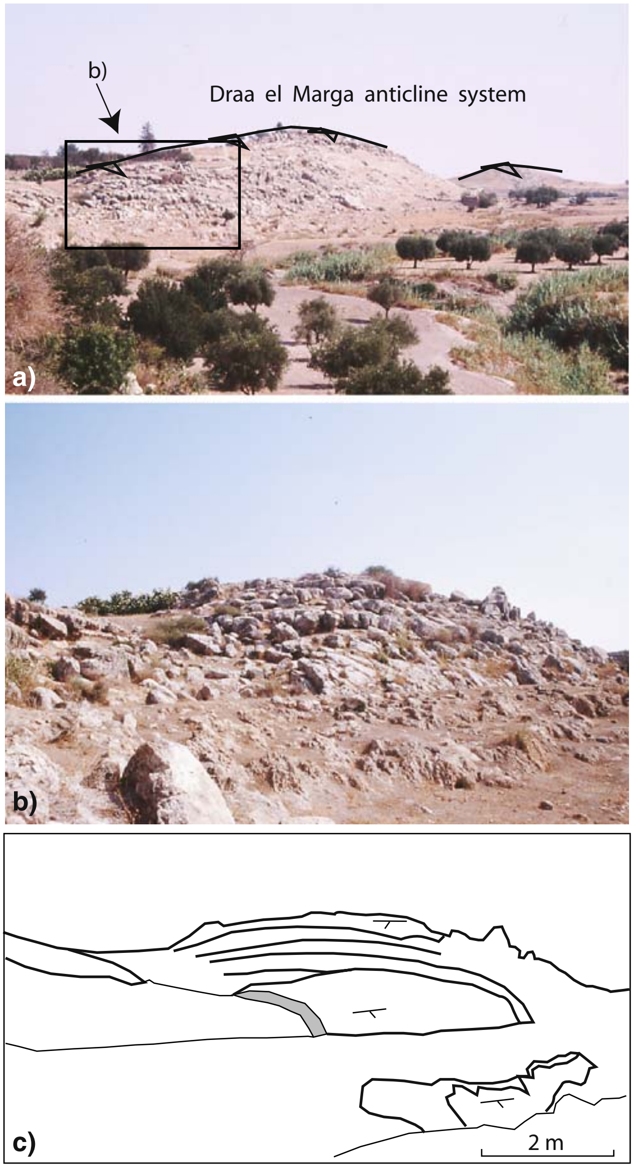

Fig. 9 Draa el Merga anticline. This structure, together with two other similarly trending anticlines, affects Late Pliocene Lacustrine limestone. For location see Figs. 2 and 5. **a** View from SW of the anticlines; **b** detail of the structure and **c** line drawing of photograph in (**b**)

top of the complex can also be evidenced. This testifies the internal deformation of the rock body (Fig. 7, section MKF13). The deformed Nappe Prerifaine as a whole was later involved in deformation, and the previously formed thrust faults were folded again.

Interesting data about both the sedimentary and structural evolution of the foredeep basin derive from the interpretation of the available seismic lines (MKF17-MKF18-MKF19, Fig. 8). Sections MKF17 and MKF19 (Fig. 8) show a gently decreasing thickness of sediment infilling towards the SE, well controlled by PBF1 well (Fig. 4), with an onlap towards the Middle Atlas foreland. The sediments are slightly deformed by the Ain Lorma normal fault system. In contrast, the transversal section MKF18 shows an increasing thickness towards the north or northeast i.e. towards the Rif chain, and one can evaluate the maximum thickness of the foredeep Meknes-Fes basin as approximately 2,000 m, also controlled through the MG-1 well. Other wells (well OR-3, Fig. 4) and seismic lines (line MKF2, Fig. 6) have confirmed a similar thickness. The poorly imaged structures affecting the Neogene and Quaternary foredeep sequence are shown close to the leading edge of Rif where the Draa el Merga structure (line MKF19, Fig. 8) coincides at the surface with the already mentioned en-echelon anticlines with ENE–WSW-trending axes affecting the Late Pliocene Lacustrine Limestones (Figs. 2, 9). Other significant deformations are displayed on lines MKF2 and MKF5 (Fig. 6). The Jebel Bou Kennfoud ridge overthrusts the Late Tortonian–Messinian foredeep sediments, which also show growing strata attesting deformation during sedimentation, allowing also a dating of the structural emplacement.

Some of the major normal faults cutting across the Hercynian basements seem to be reactivated during the later compressive tectonics although their kinematics are not clear (Figs. 6, 7).

Field structural analysis

In order to evaluate the kinematics of the major structures affecting the study area, a structural field study has been performed. The structural complexity of the area can also be seen from mesostructures, although they are not particularly abundant. The different orientations of the reconstructed stress fields are strongly dependent on the major structure they are associated with (Fig. 5; Table 1). However, they are locally well developed and unambiguous (Fig. 11), and affect different units allowing indirect control of the results. Our structural observations, as well as those done by previous authors (Faugeres 1978, 1981; Aït Brahim and Chotin 1984, 1989; Morel 1988, 1989; Moratti et al. 2003; Aït Brahim et al. 2002; Bargach et al. 2004), allow reconstructing two major compressive phases. It should also be noted that, from other structural considerations and without detailed structural analyses, Levy and Tilloy (1952), Tilloy (1955), and Choubert and Faure-Muret (1962) indirectly attained similar conclusions. These compressive phases occurred after the Mesozoic extensional and transtensional tectonics that led to the formation of the above-described graben systems.

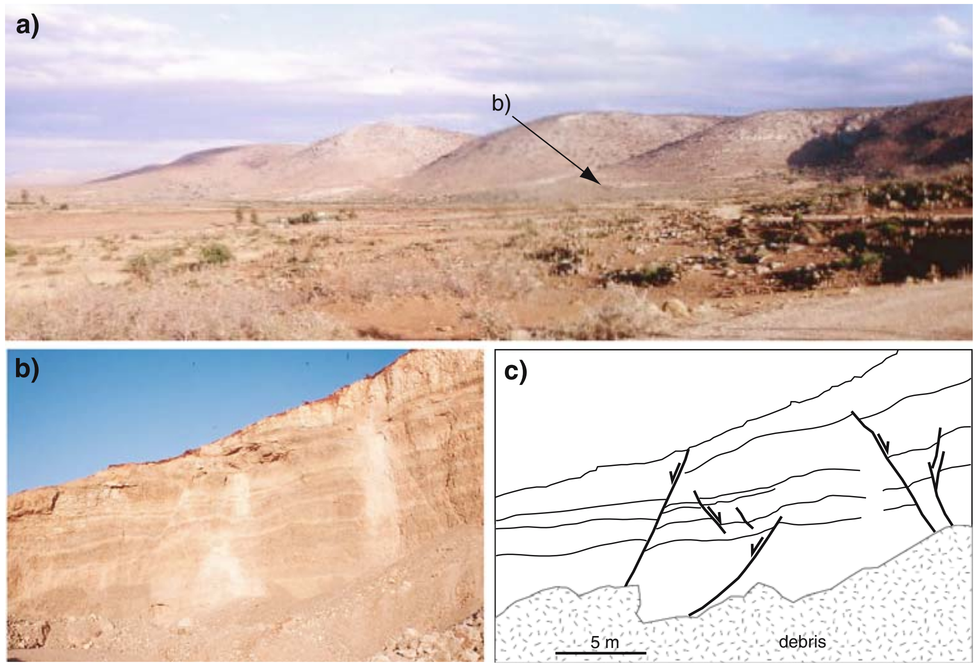

Fig. 10 **a** Panoramic view of the Ain Bittit–Ain Cheggag normal fault system delimiting the northern margin of the Middle Atlas; **b** Mesoscopic normal fault system outcropping in a quarry close to Ain Bittit and **c** line drawing of **b**. The faults affect Jurassic limestones of the Middle Atlas foreland

A first response to compressive tectonics was the formation of the foreland basins at the leading edge of the whole Rif chain during Tortonian–Messinian times (Fig. 1). The sediments that filled the basin during this phase are mainly marls (Beni Ammar White Marls and Blue Marls Fm.). The emplacement within this marly succession of the accretionary complex of the Nappe Prerifaine during the latest Tortonian–Messinian, testifies the tectonic activity of the Rif chain during this time interval (Bruderer et al. 1950a, b; Levy and Tilloy 1952; Faugeres 1978; Morel 1988; Flinch 1993; Zizi 1996a, b, 2002; Bendkik 2004; Chenakeb 2004). The maximum compression direction associated with this tectonic phase is roughly NE–SW to ENE–WSW oriented (Fig. 12; Table 1; Faugeres 1978, 1981; Aït Brahim and Chotin 1984; Morel 1988, 1989). Major structures active during this phase are the frontal ramps of the RP (see sites 7, 8, 10, 13; Figs. 5, 12). The Jurassic–Cretaceous succession was detached during this phase from the Triassic evaporites and pushed toward the SW driven by the normal faults delimiting the graben (Zizi 1996a, b, 2002). From surface data it is not clear if the basement was involved in thrusting during this phase.

The main tectonic phase during which the RP assumed their present structural setting clearly followed the emplacement of the NP, during the Pliocene (Levy and Tilloy 1952), because the Nappe Prerifaine is involved in the major structures. Since Pliocene times the maximum compression direction is roughly N–S oriented, although it may locally assume different orientations (N–S ±20; Aït Brahim and Chotin 1984; Morel 1988, 1989; Bargach et al. 2004; Figs. 5, 12, sites 1, 5, 6, 11, 12, 17, 18; Table 1).

Locally, roughly E–W (±15)-oriented compressive stress fields have also been determined (see also Bargach et al. 2004), although we are not able to establish whether they represent a well defined regional stress field connected to a particular tectonic phase. It should be noted that similar orientations of the stress field are especially concentrated along major strike–slip faults (Figs. 5, 12, sites 8, 10, 14) or in sectors within strike–slip faults. In this latter case they may simply be due to older structures rotated during later phases (Figs. 5, 12, sites 4, 9, 10).

At the leading edge of the Rif chain the Late Pliocene lacustrine limestones are involved in deformation, thus demonstrating continuous compressive tectonic activity up to very recent times (Moulay Yacoub area, Draa el Merga and Aicha Mouguetaya structure; Figs. 5, 12, site 4). Active faults have been detected in the area of Jebel Zalagh, and the associated focal mechanisms show a still active N–S-trending compressive stress field (Figs. 5, 12; Moratti et al. 2003 and references therein).

Analogue models

Even if the structural interpretation of seismic lines was able to highlight the involvement of the Palaeozoic basement in the deformation, it was not able to indicate the modalities and timing of fault reactivation.

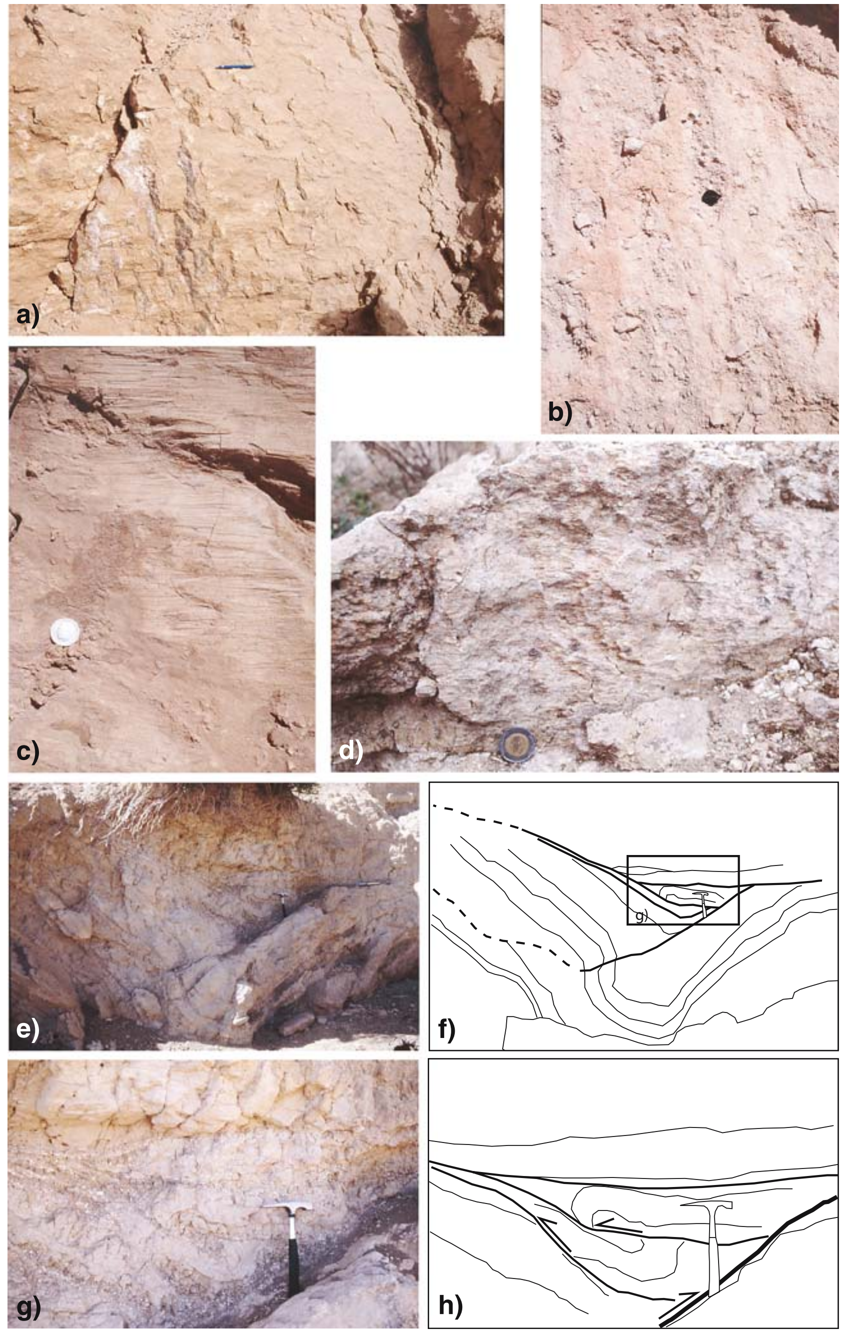

Fig. 11 Field examples of structures used for mesoscopic analysis. For site locations see Fig. 5. **a** Strike–slip fault plane at site 14, Middle-Late Miocene sandstones; **b** striated fault breccia along the frontal thrust of Jebel Kannoufa; **c** strike–slip fault plane at site 7, Jurassic limestone; **d** strike–slip stylolitic striae affecting Late Pliocene lacustrine limestone at site 3; **e** mesoscopic fold with associated contraction faults at site 13, Late Tortonian–Messinian sands and marls; **f** line drawing of photograph (**e**); **g** detail of (**e**) showing second-order folds associated with the contraction fault at the core of the major syncline; **h** line drawing of (**g**)

Many observations indicate a strike–slip activity along faults affecting the cover and running parallel to the Mesozoic normal fault systems. Two alternative hypotheses for the RP evolution and emplacement can be suggested: (a) in the context of the collision between Africa and Europe, the RP thrust décollement system may be interpreted as a ‘‘scooped-out graben fill’’ transported towards the SW without reactivating the Hercynian ‘‘basement’’ (Zizi 1996a, b, 2002) or alternatively: (b) the compression (convergence) between Africa and Europe may have led to a reactivation of the favourably oriented faults within the basement according to the main compressive stress axis (roughly N–S oriented since Pliocene); this caused the thrusting to the SW as well as the transpressive reactivation of the previous normal fault systems to which the salt tectonics are also related.

Given these uncertainties about the interpretation of these structures, we carried out a series of analogue modelling experiments to investigate the role of the basement during deformation. Although analogue modelling necessarily involves important

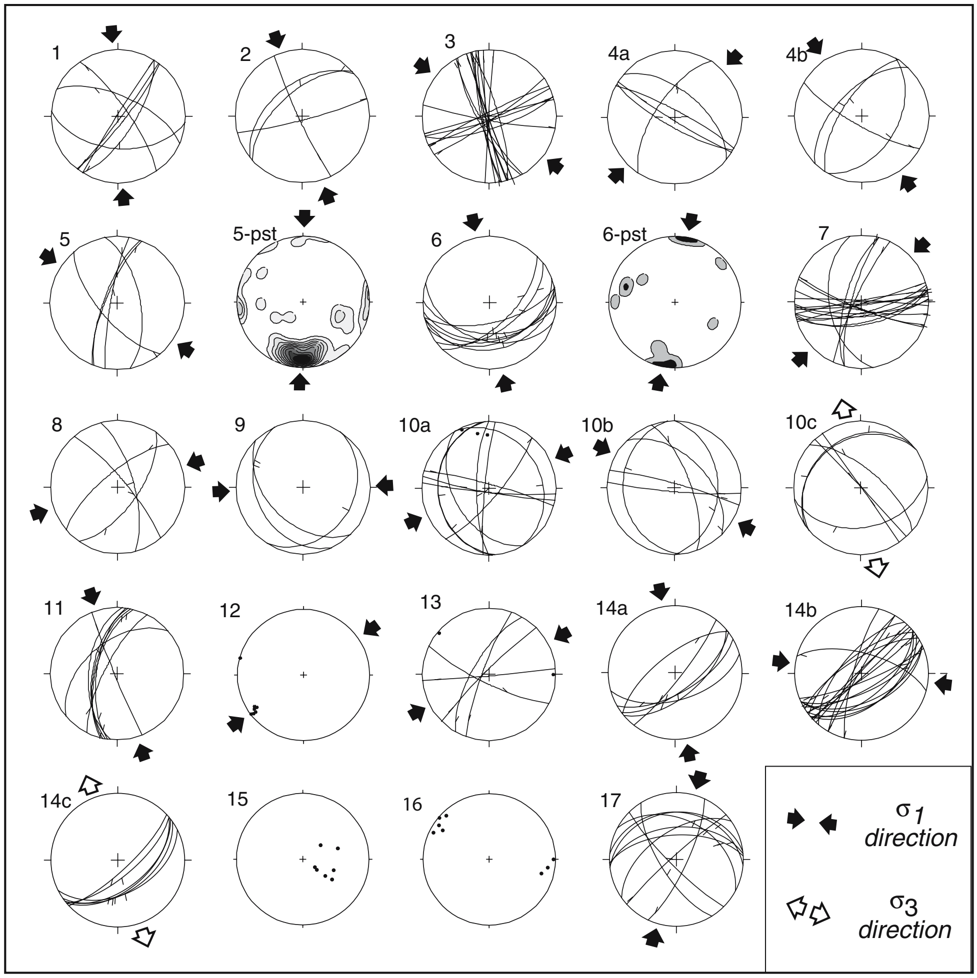

Fig. 12 Stereo plots of mesoscopic structural data (Schmidt projection, lower hemisphere). Fault planes are represented by *great circles* and fold axes by *black points*. Density diagrams of solution pits are represented for sites 5 and 6 (*5-pst* and *6-pst*, respectively). Palaeostress orientations of fault-slip data have been computed using the Carey (1979) inversion method, whereas for mesoscopic fold axes and stylolithic pits on pebble surfaces the main shortening direction has been estimated. The site number is indicated *beside* the stereo plots and their locations are reported in Fig. 5. The results are summarized in Table 1

simplifications, it is commonly accepted that first order model results are not invalidated by such limitations (e.g. Brun 1999), and give useful hints in analysing the deformation mechanisms. Analogue models were performed at the ''Tectonic Modelling Laboratory'' of the Department of Earth Sciences in Florence (Italy). The models were scaled to correctly reproduce the natural prototype satisfying the geometric, rheologic, kinematical and dynamic similarities (e.g. Hubbert 1937, Ramberg 1981; Weijermars and Schmeling 1986; Weijermars et al. 1993; Brun 1999; table in Fig. 13; Table 2).

Model construction and deformation

The analogue models were built and deformed following the structural evolution of the study area. In particular the models are deformed through different phases. In this paper we present two models deformed under two phases (both belonging to a larger experimental series performed to study the effects of different orientations of shortening on reactivation of earlier normal faults systems; Del Ventisette et al., 2006, in press) and new models deformed under three different phases. Through these models it was possible to understand the role of early normal faults during later phases of shortening.

The models, with initial dimensions of 45.5 cm × 42 cm × 7 cm, were run using a pure–simple shear deformational apparatus (Fig. 13) with dimensions such that 1 cm in the model represents 1 km in nature, allowing to investigate in detail the model deformation patterns. To evaluate the possible strike–slip reactivation of the earlier extensional normal faults affecting the basement during the successive compressive phase we also inserted 3.5 cm-wide sand bands with different colours parallel to the extension direction (Coloured Marker Layer; CML; Fig. 13).

During the first deformation phase the models were extended at a constant velocity of 10 mm h^{-1} for 7 h up to a bulk extension (BE) of about 16.5%. This phase simulates Triassic–Jurassic tectonics, leading to the formation of NE–SW striking graben structures. During this phase the syn-tectonic sedimentation has

Table 1 Mesoscopic structural field data of the Meknes-Fes Basin

Sites	Kind of structures	Number of data	σ_1 az/dip	Computed σ_2 az/dip	σ_3 az/dip	Estimated mean shortening direction	Unit or formation	Age of deformed rock
1	Faults	7	356/1	87/50	265/40		Lacustrine limestone	Late Pliocene
2	Faults	4	325/5	255/45	73/44		Lacustrine limestone	Late Pliocene
3	Faults	19	312/10	191/85	27/5		Lacustrine limestone	Late Pliocene
4a	Faults	5	225/3	329/12	142/78		Lacustrine limestone	Late Pliocene
4b	Faults	4	326/10	233/18	83/70		Lacustrine limestone	Late Pliocene
5	Faults	5	304/16	183/61	42/23		Sablefauves	Pliocene
5	Solution pits	69				182/5	Sablefauves	Pliocene
6	Faults	9	170/6	253/1	43/89		Blue marls	Late Tortonian –Messinian
6	Solution pits	14				190/2	Blue marls	Late Tortonian –Messinian
7	Faults	17	47/14	242/75	137/3		Limestone	Jurassic
8	Faults	4	72/30	300/50	180/21		Limestone	Jurassic
9	Faults	3	88/7	179/14	350/75		Lacustrine limestone	Late Pliocene
10a	Faults and folds	10 + 3	246/11	156/8	26/77	255/10	Limestone	Jurassic
10b	Faults	6	299/1	207/66	29/24		Limestone	Jurassic
10c	Faults	6	252/65	78/23	167/10		Limestone	Jurassic
11	Faults	7	162/10	253/23	89/63		Sandstones	Middle Miocene
12	Solution pits	7				235/5	Lacustrine limestone	Late Pliocene
13	Faults and folds	5 + 2	242/18	339/39	142/49	210/5	Blue marls	Late Tortonian –Messinian
14a	Faults	6	170/9	77/23	280/65		Sandstones	Middle Miocene
14b	Faults	19	98/12	15/70	13/15		Sandstones	Middle Miocene
14c	Faults	7	283/67	60/17	155/15		Sandstones	Middle Miocene
15	Folds	7					Limestone	Jurassic
16	Folds	8				24/5	Lacustrine limestone	Late Pliocene
17	Faults and folds	10 + 3	196/16	298/35	85/50	227/10	Lacustrine limestone	Late Pliocene

Palaeostress orientation of fault-slip data has been computed using the Carey (1979) inversion method, whereas from mesoscopic folds axes and stylolithic pits on pebble surfaces the main shortening direction has been estimated. Location of sites is shown in Fig. 5

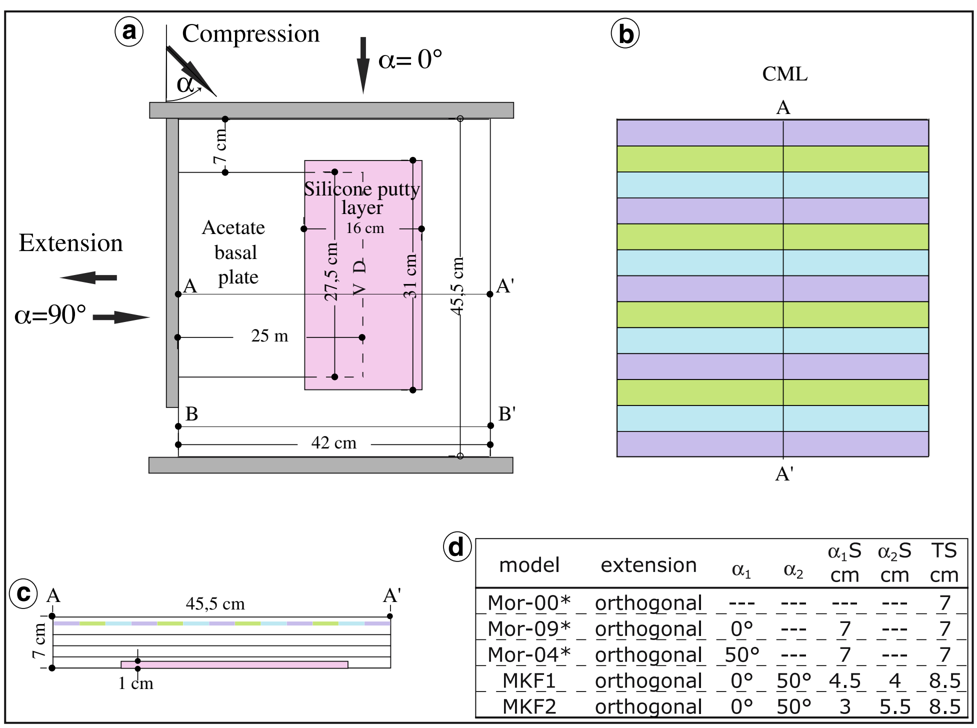

Fig. 13 Model set-up: **a** Plan view illustrating the position of the basal acetate plate and of the silicone putty layer; *VD* velocity discontinuity. *Black arrows* indicate direction of extension and compression, respectively. The models were set up on an acetate basal plate fixed to the moving wall (on the *left*) producing a VD at the base of the models during extension; **b** Plan view of model before deformation. Note the *coloured* markers which allow detecting strike–slip components along reactivated faults. **c** Cross-section across the model. **d** Table with analogue model parameters and scaling ratios

been reproduced and, according to the scaled natural lithology of the sediments in the study area, it is composed of a basal layer of silicone putty (simulating the ductile Late Triassic–Early Jurassic evaporites) overlain by dry quartz sand sieved at regular time intervals on top of the models (simulating the essentially brittle syn-rift sediments; Table 2). The final thickness of the syn-kinematic sand panel inside the graben was of the order of 3 cm corresponding to 3 km in nature (Fig. 13d). This phase is equal in bulk extension and in velocity for all the performed experiments. At the end of this first extensional phase a thin black layer of dry sand was sieved on the surface of the models. A grid of passive markers was drawn onto the model to show the fault offsets during the second deformation phase.

The following deformation phases, simulating a compressive stress field, were applied at the constant velocity of 10 mm h^{-1} for 7 h giving a total shortening of about 7 cm. During this phase the models were shortened varying the angle between the direction of the maximum horizontal stress axis (σ_1) and the trend of main normal faults delimiting the graben formed during the first extensional phase. This angle (called obliquity angle and labelled with α) was varied between 0° and 90° [see Del Ventisette et al. (2006, in press) for details about the complete series]. In the study area the graben systems actually trend in a roughly NE–SW direction, whereas the directions of compression were around NE–SW directed during the Late Tortonian phase and around N–S trending during the Pliocene–Quaternary phase. These orientations allow us to select for this paper the models with obliquity angle $\alpha = 0$ and 50°, respectively, as particularly useful and representative to investigate the natural prototype. For a complete and more detailed description of the experimental procedure and of the results of the entire series refer to Del Ventisette et al. (2006, in press).

During deformation top-view photographs of the models were taken at regular time intervals to investigate the time–space evolution of structures. At the end of the experiments, dry sand was sieved on the model surfaces to preserve the final topography. Then models were wetted and serial cross-sections were cut perpendicular to the graben axis approximately every 2 cm allowing the reconstruction of the three-dimensional final deformation pattern.

To describe in detail the effects of the first extensional phase, we deformed a test model (model Mor-00) only in extension but with the same BE and strain rate of the models deformed also with shortening. Top-view photographs of this model show the same structural features observed at the end of the extensional phase in the other models, demonstrating the reproducibility of the model set-up (Del Ventisette et al., 2006, in press). In particular, after the extensional phase a single and near-symmetrical graben formed with a maximum depth of about 4 cm delimited by two transfer zones developed in correspondence of the upper and lower transversal borders.

To observe the effects of the compressive phase onto the previously formed graben, we deformed the models through a stress field with the maximum compressive axis parallel to the graben axis ($\alpha = 0$) and another model with maximum compressive axis with an obliquity angle α of about 50° with respect to the graben axis. These stress fields have the same orientation, with respect to the graben setting, as those acting during the Late Tortonian and Pliocene–Pleistocene times, respectively. Moreover, to better reproduce the

Table 2 Analogue modelling parameters

	Model	Nature	Model/nature ratio
Parameters			
BL density, ρ_{bsk} (kg m^{-3})	1,300	2,600	0.5
BL friction coefficient, μ_{bsk}	≈0.8		
DL (salt) density, ρ_{dsk} (kg m^{-3})	1,060	2,200	≈0.5
DL (salt) viscosity, η_{dsk} (Pa s)	10^3	5×10^{17}	2×10^{-15}
Scaling parameters			
Strain rate, ϵ (s^{-1}) $\epsilon^* = \sigma^*/\eta^*$			3.4×10^9
Gravity acceleration, g (m s^{-2})	9.81	9.81	1
Length, l (m) $l^* = l_{mod}/l_{nat}$	0.01	1,000	1×10^{-5}
Stress, σ (Pa) $\sigma = \rho\ g^*\ l^*$			4.8×10^{-6}
Time, t (s) $t^* = 1/\epsilon^*$	3,600	1.3×10^{13} (≈0.4 Ma)	~2.8×10^{-10}
Rate of displacement, v (m s^{-1}) $v^* = \epsilon^*\ l^*$	2.7×10^{-6}	7.9×10^{-11} (2.5 mm $year^{-1}$)	3.4×10^4
Syn-tectonic sedimentation rate (m s^{-1})	5.5×10^{-7}	1.6×10^{-11} (0.58 mm $year^{-1}$)	3.4×10^4

The asterisk indicates the ratio between the model and the natural prototype. *BL* brittle layer, *DL* ductile layer (the model ductile layer is constituted by silicone and oleic acid) observed natural case as described in the previous chapters, we performed also a model in which the early extensional phase was followed by two compressive phases through time.

Experimental results

In this section we first present the results obtained from the models deformed under one phase of shortening (models Mor-04 and Mor-09, Fig. 14) to explain the relationship between the final structural pattern and the direction of shortening. Then, we present the results of the models deformed during two successive phases of shortening (models MKF1 and MKF2).

Shortening parallel to the graben axis (α = 0°)

In this model (model Mor-09, Fig. 14a), roughly reproducing the stress field affecting the area during the Late Tortonian phase, the structural pattern in map-view is characterized by two major thrust-décollements localized within the graben and trending orthogonal to its axis. These structures developed in response of the marked decoupling of the basin fill from the basement (Fig. 14a). This decoupling is also evidenced by the doubling of the sedimentary cover in correspondence to the syn-tectonic ductile layer (Fig. 14a, cross-sections 1, 2). This thin-skinned tectonics within the graben created the typical final deformation geometries frequently recognized in natural inverted grabens (i.e. Morley et al. 2001, 2003). Another important feature of the final deformation pattern is the newly formed thrust fault, trending orthogonal to the direction of compression, cutting across the whole model (Fig. 14a). This structure clearly affects the graben shoulders, whereas its propagation into the basin is more complex because it interferes with both the pre-existing normal faults, reactivated as tear faults, and with the structures emanating from the ductile layer at the graben fill-basement interface. The pre-existing normal faults are generally reactivated with strike–slip kinematics, as displayed by the deformation of the passive grid on the model surface (Fig. 14a, cross-section 1). The basement faults show also a dip-slip component of reactivation at least for the uppermost segment of the fault bounding the syn-tectonic basin fill (Fig. 14a). Moreover, although this model is deformed under a shortening direction trending parallel to the graben axis, the graben border faults also reactivated with a dip-slip component of movement (e.g. see the border fault on the left in cross-section 2 in Fig. 14a).

Shortening phase with α = 50

The model with shortening at α = 50 (model Mor-04; Fig. 14b) shows in map view a very complex structural setting developed through time. After 2 h of deformation two major thrust faults developed at the graben margins (Fig. 14b). After 4–6 h, arcuate thrust faults developed partly starting from the previous ones. Other structures, oriented roughly perpendicular to σ_1, developed as well. The final configuration (after 7 h of deformation; Fig. 14b) results, in map-view, in a very complex structural pattern with faults variably oriented and connected by minor strike–slip faults. Moreover, the lower part of the basin appears to be ‘‘extruded’’ developing out-of-the-graben-like structures. Also in this model the early normal faults are reactivated during the shortening phase. Comparing final top view and cross-sections, the strike–slip reactivation appears less developed in the sedimentary cover than in the basement. In detail, the grid on top of the model shows very small dislocations, whereas the juxtaposition of the different colours of the CLM level are evident in cross-sections (Fig. 14b, cross-sections 3, 4). In the central part of the graben a double-vergent structure is characterized by a pop-up-like geometry with silicone uprising at the core (Fig. 14b, cross-section 5). This geometry of deformation may be related either to a change of the vergence of this structure during deformation or to a pre-existing discontinuity (formed during the first extensional phase of deformation) with contemporaneous development of the double-vergence (Fig. 14b cross-sections 4–6). Dislocation of both the CML and the top-surface grid allows reconstructing the strike–slip movements of structures both in the basement and in the basin fill. In the central part of the model (Fig. 14b) the strike–slip component of the movement is left lateral for the most internal fault and right lateral for the most external fault. In addition, whereas the grid onto the model highlights a right-lateral displacement, the change of colours of the CML gives instead a left-lateral dislocation for the basement faults. This behaviour in this model also may again indicate a strong decoupling between basement and sedimentary cover.

In both the discussed models, the major extensional faults are invariably reactivated during the compressive phase. For α = 0 pre-existing structures acted prevalently as dislocation zones and tear-faults for newly formed thrusts. For α = 50° the strain is instead mostly accommodated by reactivation of pre-existing structures.

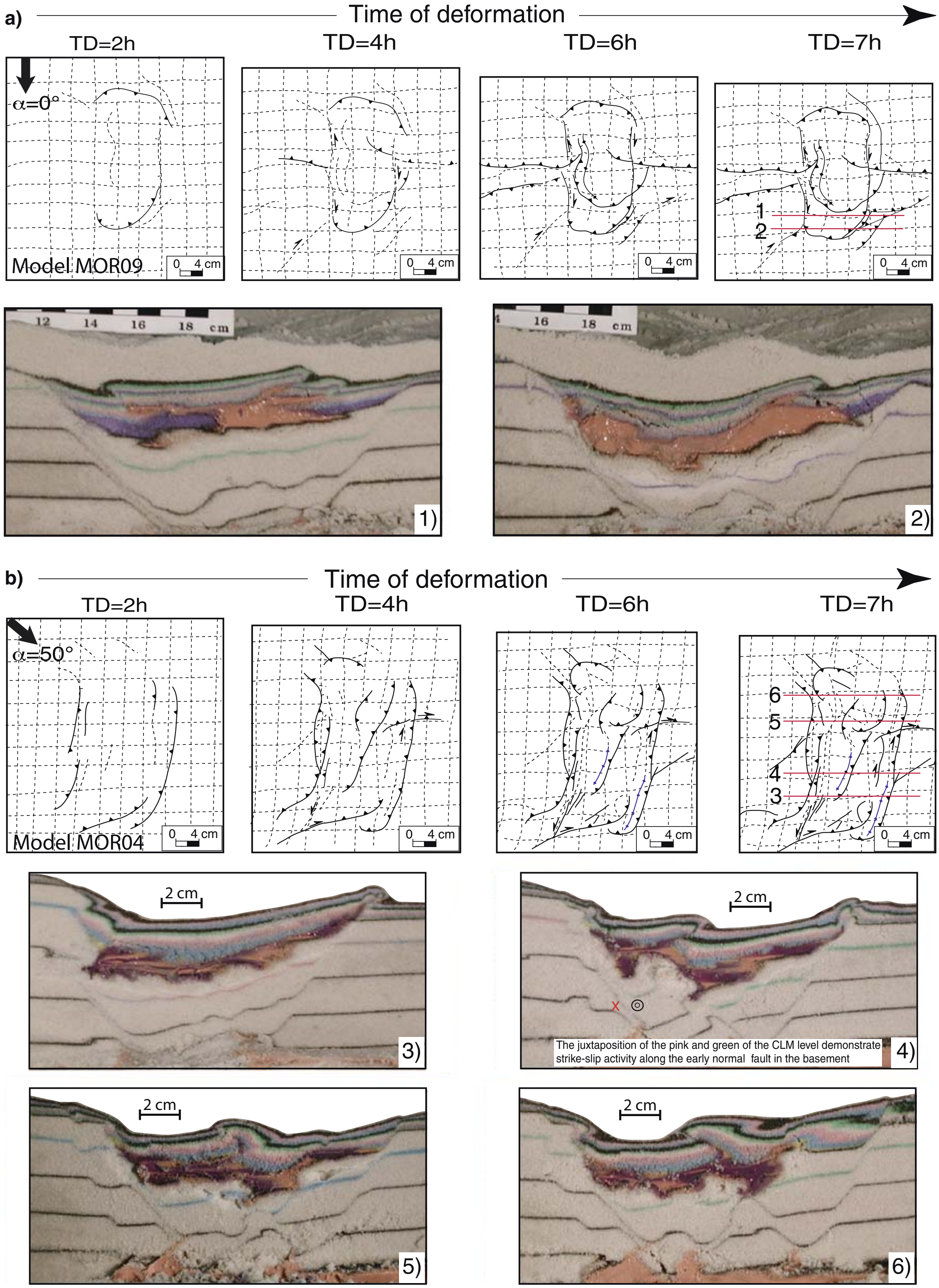

Fig. 14 **a** Model MOR09 (α = 0) illustrating compressive deformation parallel to the graben axis. Top views of model after 2, 4, 6, and 7 h of deformations, respectively. The final drawing (after 7 h) shows the location of cross-sections 1 and 2, which are reported below. **b** Model MOR04 (α = 50) illustrating compressive deformation at 50° to the graben axis. Top views of model after 2, 4, 6, and 7 h of deformations, respectively. The final drawing (after 7 h) shows the location of cross-sections 3–6, which are reported below

Shortening with α varied from 0° to 50° during deformation

Since Late Tortonian, the studied sector of Morocco underwent two different successive compressive phases characterized by different stress field orientations. This evolution implies that structures formed during different deformation phases were possibly re-used (or even inverted) during later phases of deformation. To better investigate the role and influence of pre-existing compressive structures on localization and final geometry of the RP, we performed two further new models (MKF1 and MKF2) deformed under the same boundary conditions but with different bulk shortening (see Fig. 13d). In these experiments, after the extensional phase, the following shortening was characterized by different orientations of σ_1. The obliquity angle α was varied from 0° to 50° according to the variation of the stress field orientation determined from structural data that show a compressive phase with a roughly NE–SW-trending σ_1 followed by a still active phase with a N–S-trending σ_1.

The models displayed a similar evolution, so that the results of the model MKF2 have been chosen as representative. The deformation pattern at the end of the first compressive phase (α = 0) shows important reactivations of the structures inherited from the extensional phase (Fig. 15a). Along the transfer zones delimiting the graben, the deformation is strongly localized and characterized by structures detached from the décollement level. These décollements, simulating the natural Triassic evaporites, strongly favoured the scooping out of the graben fill. At the same time reverse faults developed also on the graben shoulders.

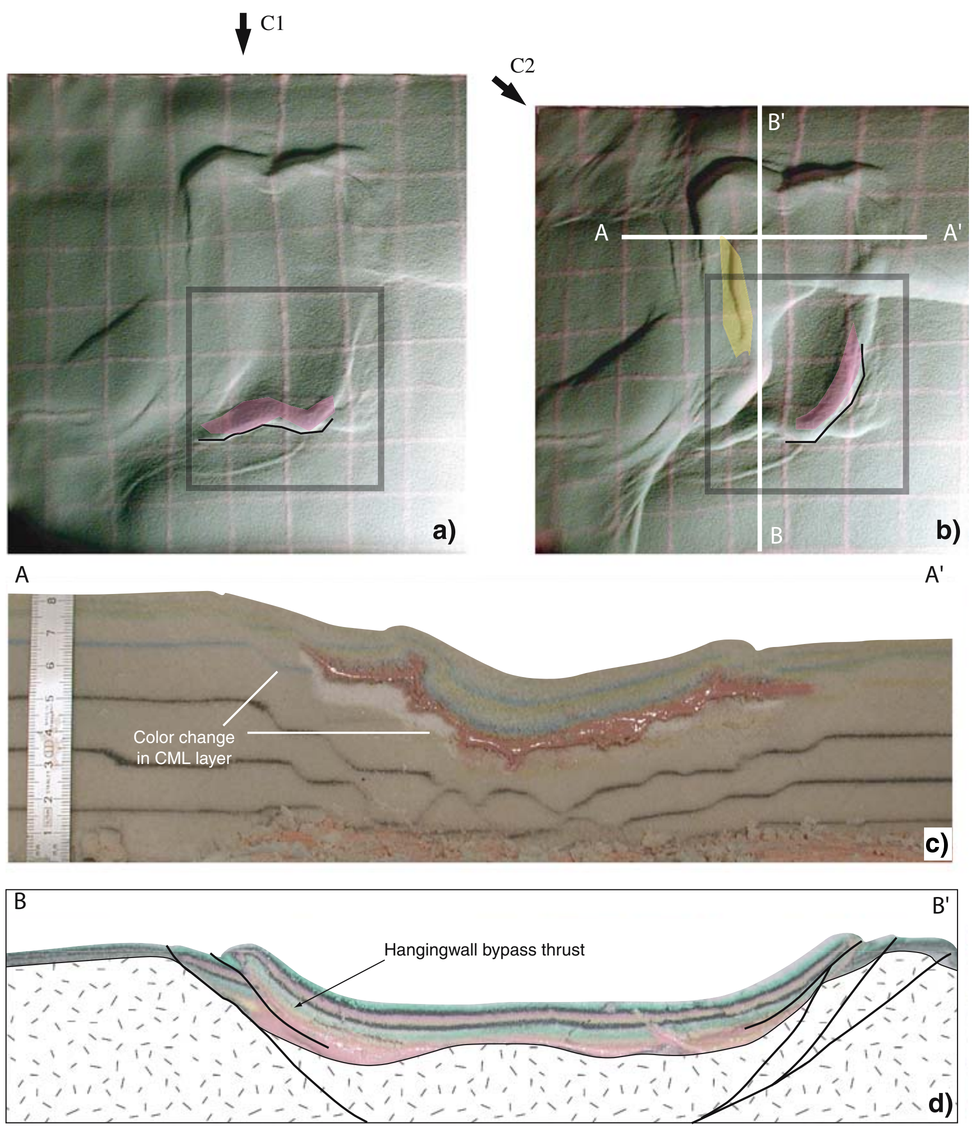

Fig. 15 Model MKF2 reproducing the extensional phase followed by two compressive phases with different σ_1 orientations parallel (*top view* in **a**) and at 50° (*top view* in **b**) to the graben axis, respectively; **c** cross-section of model at the end of deformation (see location in **b**). Note the different *colours* of CML indicating a strike–slip reactivation of earlier basement normal faults; **d** section parallel to the graben axis; the hanging wall bypass thrust is also indicated. For further comments see text

During the second compressive phase ($\alpha = 50$; Fig. 15b) the structures already reactivated during the first phase are further enhanced demonstrating the importance of localization of deformation during inversion tectonics. The top view of the model at the end of the experiment (Fig. 15b) shows a very complex deformation pattern whose major feature is the sinuosity of thrust faults, being strongly controlled by the trends of buried earlier normal faults and by the thrust faults developed during the first compressive phase. As a consequence, some segments of thrust faults are not or less active whereas, in contrast, some other segments are more active or strongly enhanced during this phase.

The model cross-sections also show a strong strike–slip component of reactivation of the basement faults

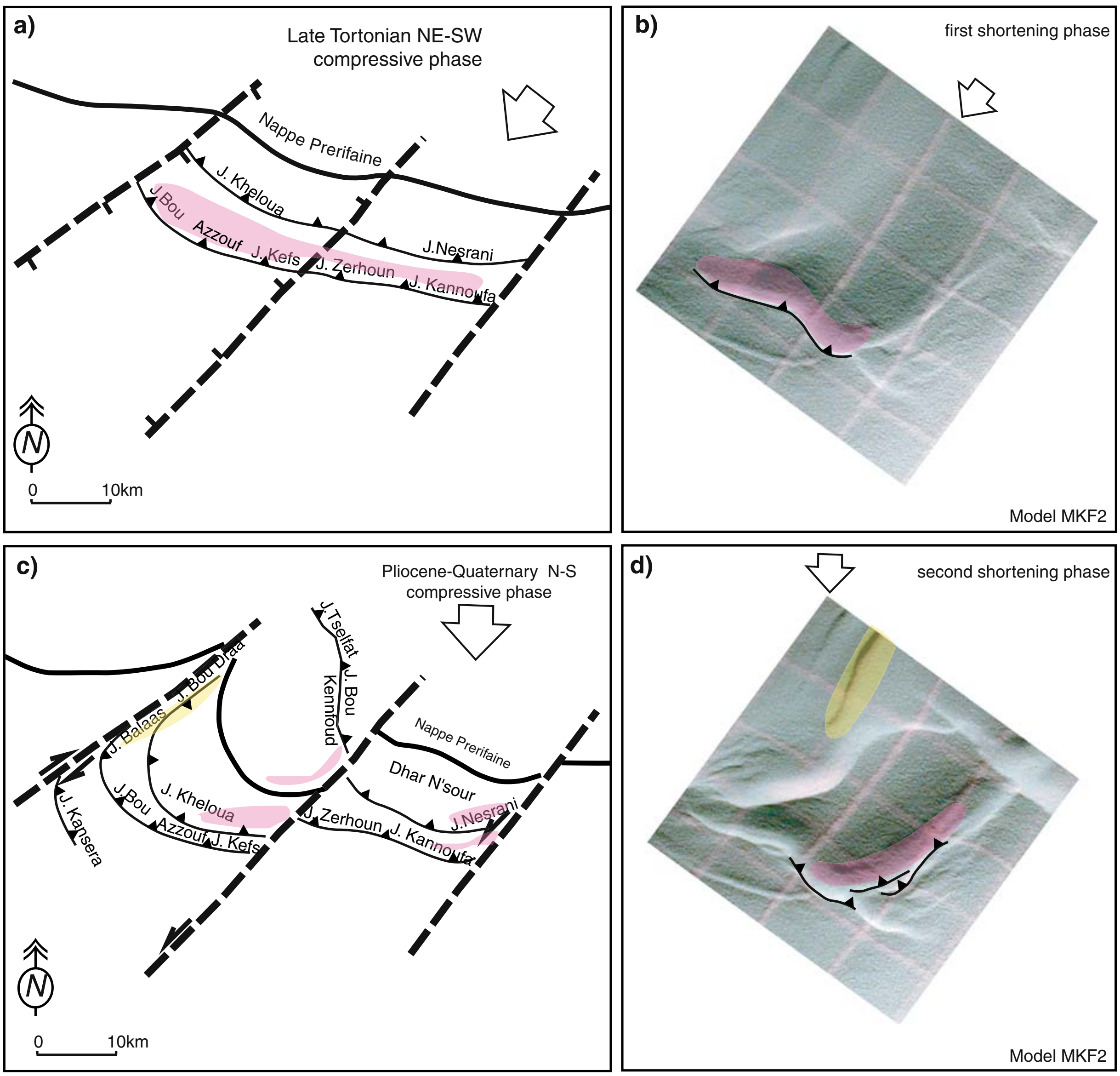

Fig. 16 Evolutionary model of the Rides Prerifaines (RP) and comparison with model top-views. **a** During Late Tortonian the first compressive phase is characterized by a NE–SW-trending σ_1. The Nappe Prerifaine advanced and reached the foredeep. The basin fill was detached from the Triassic evaporites and scooped out towards the SW. Mesozoic normal fault systems drove the thrusts' leading edge; **b** the top view of the model roughly reproduces this situation of a developing frontal thrust, corresponding to the scooped-out basin fill detached at the base (i.e. silicone layer); **c** The Pliocene–Quaternary, N–S-trending compressive phase reactivated both the Mesozoic normal fault systems and the thrust faults developed during the Late Tortonian compressive phase. This is confirmed by the strike–slip component detected along the earlier normal fault affecting the basement and by the strongly arcuate trends of thrust faults typically characterizing the RP; **d** the model top-view confirms this evolution giving rise to a newly formed thrust front, or reactivating the older ones, increasing their throw

particularly well evidenced by the change in colour of the CML level across the fault (Fig. 15c, cross-section A–A′).

The section parallel to the graben axis in the model MKF1 (Fig. 15d), similar to the model MKF2, clearly shows structures formed in correspondence to the early formed transfer faults. In particular, a well-developed hanging wall by-pass thrust propagating from the ductile level produces the scooping out of the graben fill

Discussion and conclusions

The integration of structural field studies with seismic line interpretations and the comparison with the experimental results, allow proposing a model on the evolution and the formation of the RP through time.

As a more general frame, we may suggest that the normal fault systems laterally constrained and strongly conditioned the thrusting processes of the RP, which detached from the Triassic evaporites, also giving rise to salt tectonics particularly evident on seismic profiles along the NE–SW faults (Figs. 6, 7). The following compressive phases that affected the study area had different effects on the dynamics of deformation and their interference gave rise to the current setting, characterized by a strongly arcuate shape of thrust faults in map view.

The first compressive phase acted since Late Tortonian with a NE–SW-oriented σ_1, i.e. roughly parallel to the axes of the Mesozoic grabens. The Triassic evaporites favoured the detachment from the Palaeozoic basement and frontal ramps corresponding to thrust anticlines formed, currently represented by Jebel Bou Azzouf–Jebel Kefs and Jebel Zerhoun–Jebel Kannoufa (Fig. 16a). The Nappe Prerifaine trend during this phase has been supposed as roughly linear. For this first phase the interpretation of a scooped-out graben fill is very likely (Zizi 1996a, 2002). This deformation gave rise to mainly frontal structures, with poor or negligible strike–slip reactivation of major normal faults affecting the basement at depth and delimiting the graben structures (Fig. 14a).

During the second compressive phase characterized by a roughly N–S-trending σ_1 (corresponding to $\alpha = 50$), which acted since Pliocene times and which is still active, the RP assumed their present setting. The analogue model results suggest that with the progression of deformation and particularly for angles of α around 50° the reactivation of early normal faults in the basement is favoured. As a consequence, in the studied case, under the Pliocene stress field a strike–slip reactivation along major basement fault systems is expected to occur and not during the Late Miocene stress field. During this phase a general shortening of the area took place and ridges developed roughly parallel to the major Mesozoic normal faults of the area like the Jebel Bou Draa–Jebel Balaas, Jebel Tselfat–Jebel Bou Kenfoud and Jebel Nesrani (Fig. 16b). Frontal ramps were also active during this phase. The orientation of the stress field implies that they are nearly parallel to the major Mesozoic normal faults. The activity along the currently lateral ridges is enhanced by the strike–slip reactivations of the normal faults affecting the basement, which inverted their kinematics and also promoted salt tectonics (Nzala des Oudayas) and fluid circulation and migration (e.g. Sidi Fili oil field). The previously emplaced NP is again involved in deformation during this second phase. The Nappe Prerifaine is clearly imaged on seismic lines, buried below Late Miocene sediments. It also crops out at surface where its leading edge is eroded, or it is cut by strike–slip faults along the major fault systems.

The complex structural pattern displayed on the geological map as well as in the seismic lines may represent the results of the interference of the above-described processes of deformation. Moreover, comparison between structural styles reproduced in models of Figs. 14 and 15 with that imaged on seismic lines (Figs. 6, 7, 8) confirms the reliability of the analogue modelling approach.

Acknowledgments This work strongly benefited from the discussion with Prof. A. W. Bally, who is warmly thanked also for making available a lot of material about the area. ONAREP (now ONHYM) is also thanked for providing seismic sections and well logs studied and illustrated in this work. Dr. M. Dahmani, past Director of the Geological Survey of Morocco, is warmly acknowledged for his help during fieldwork years and for useful suggestions. Useful discussion in the field with M. Boccaletti, R. Gelati, G. Moratti and G. Papani greatly improved the paper. Anonymous referees and Prof. R. Greiling are also thanked for their help in improving the manuscript. Field work was funded by Italian Consiglio Nazionale delle Ricerche (CNR), Ministero dell'Università e della Ricerca (MIUR) and by the bilateral project between CNR (Italy) and CNRST (Morocco) ''Structural analysis, active tectonics and fluids geochemistry in the Rif-Middle Atlas-High Atlas System of Morocco'' (Italian responsible Dr. G. Moratti)

References

Aït Brahim L, Chotin P (1984) Mise en évidence d'un changement de direction de compression dans l'avant-pays rifain (Maroc) au cours du Tertiaire et du Quaternaire. Bull Soc Géol Fr Ser 7(26):681–691

Aït Brahim L, Chotin P (1989) Genèse et déformation des bassins néogènes du Rif central (Maroc) au cours du rapprochement Europe-Afrique. Geodinamica Acta 3:295–304

Aït Brahim L, Chotin P, Hinaj S, Abdelouafi A, El Adraoui A, Nakcha C, Dhont D, Charroud M, Sossey Alaoui F, Amrhar M, Bouaza A, Tabyaoui H, Chaouni A (2002) Paleostress evolution in the Moroccan African margin from Triassic to Present. Tectonophysics 357:187–205

Bargach K, Ruano P, Chabli A, Galindo-Zaldivar J, Chalouan A, Jabaloy A, Akil M, Ahmamou M, Sanz de Galdeano C, Benmakhlouf M (2004) Recent tectonic deformations and stresses in the frontal part of the Rif Cordillera and the Saïss Basin (Fes and Rabat regions, Morocco). Pure Appl Geophys 161:521–540

Bendkik A (2004) Carte Géologique du Maroc, Feuille Sidi Kacem, echelle 1:50.000. Notes Mém Serv Géol Maroc 431

Bernini M, Boccaletti M, Moratti G, Papani G (2000) Structural development of the Taza-Guercif Basin as a constraint for the Middle Atlas Shear Zone tectonic evolution. Mar Pet Geol 17:391–408

Bettelli G, Vannucchi P (2003) Structural style of the offscraped Ligurian oceanic sequences of the Northern Apennines: new hypothesis concerning the development of mélange block-in-matrix fabric. J Struct Geol 25:371–388

Bourcart J (1932) La Ride Prérifaine d'El Kansera (Maroc). Boll Doc Géol Fr Ser 5(2):221–236

Boutakiout M (1990) Les foraminifères du Jurassique des Rides Sud-Rifaines et des régions voisines (Maroc). Doc des Lab Géol Lyon 112:1–247

Bruderer W, Levy RG (1954) Considerations sur la ''Nappe Prerifaine'' d'apres les travaux de la Societè Cherifienne des petroles Congres Geologique International Alger XIX session, Association des Services Geologiques Africains. Deuxieme partie—Questions Diverses et annexes-Fascicule XX:277–294

Bruderer W, Delga G,Gouskov N, Gubler J, Lardenois E, Levy RG, Marquis Ch, Mourou C, Naif R, Nouet G, Ramette C, Tenaille M (1950a) Carte géologique régulière du Maroc au 1:100.000éme. Feuille Petitjean. Notes Mem Serv Géol Maroc 108

Bruderer W, Gouskov N, Gubler J, Jacquemont P, Levy RG, Tilloy R (1950b) Carte géologique régulière du Maroc au 1:100.000éme. Feuille Fés-ouest. Notes Mem Serv Géol Maroc 109

Brun JP (1999) Narrow rifts versus wide rifts: inferences for the mechanics of rifting from laboratory experiments. Philos Trans R Soc Lond A 357:695–712

Burger J-J, Housse B, Levy R (1962) Contribution des travaux d'exploration de la Société Chérifienne des Pétroles a la connaissance de la Nappe Prérifaine. Livre Mém Fallot Mém Geol Fr 1:423–430

Carey E (1979) Recherche des directions principales des contraintes associees au jeu d'une population de failles. Rev Geol Dyn Geogr Phis 21:57–66

Carte Géologique du Maroc (1985) Royaume du Maroc, Ministère de l'Energie et des Mines, Direction de la Géologie. Publ. 260 du Service Géologique du Maroc (scale 1:1,000,000)

Chenakeb M (2004) Carte Géologique du Maroc, Feuille Beni Ammar, echelle 1:50.000. Notes Mem Serv Géol Maroc 428

Choubert G, Faure-Muret A (1962) Evolution du domaine atlasique marocain depuis les temps paléozoiques. Livre Mém Fallot Mém Geol Fr 1:447–527

Costagliola A, El Alji M, Jabour H, Degnati A (1997) Middle Atlas and High Atlas Geotraverse. Field trip guidebook, Peri-Tethys Program-Onarep, Rabat, 13–15 June 1997, pp 1–88

Daguin F (1927) Contribution à l'étude géologique de la région Prérifaine (Maroc septentrional). Notes Mém Serv Géol Maroc 1:1–413

Del Ventisette C, Montanari D, Bonini M, Sani F (2005) Positive fault inversion triggering 'intrusive diapirism': an analogue modelling perspective. Terra Nova, vol 17. DOI 10.1111/j.1365–3121.2005.00637.x

Del Ventisette C, Montanari D, Bonini M, Sani F (2006) Basin inversion and fault reactivation in laboratory experiments. J Struct Geol (in press)

Faugères J-C (1978) Les rides sud-rifaines. Evolution sedimentaire et structurale d'un bassin atlantico-mésogéen de la marge africaine. These Doct. Etat. Univ. Bordeaux, pp 1–480

Faugères J-C (1981) Évolution structurale d'un bassin atlantico-mésogéen de la marge africaine: les rides sud-rifaines (Maroc). Bull Soc Géol Fr 23:229–244

Faure Muret A, Morel JL (1992) Carte Néotectonique du Maroc 1: 100.000. Feuille 1: Provinces du Nord. Notes Mem Serv Géol Maroc 368

Feinberg H (1986) Les series tertiaires des zones externes du Rif (Maroc). Notes Mém Serv Géol Maroc 315:1–192

Flinch JF (1993) Tectonic evolution of the Gibraltar Arc. Ph.D. Thesis, Rice University, Houston, pp 1–381

Flinch JF (1996) Accretion and extensional collapse of the external Western Rif (Northern Morocco). In: Ziegler PA, Horvath F (eds) Peri-Tethys Memoir 2: Structure and prospects of Alpine basins and forelands. Mém Mus Natn Hist Nat 170:61–85

Frizon de Lamotte D, Crespo-Blanc A, Saint-Bézar B, Comas M, Fernàndez M, Zeyen H, Ayarza P, Robert-Charrue C, Chalouan A, Zizi M, Teixell A, Arboleya M-L, Alvarez-Lobato F, Julivert M, Michard A (2004) TRANSMED Transect I. In: Cavzza W, Roure F, Spakman W, Stampfli GM, Ziegler PA (eds) The TRANSMED Atlas—the Mediterranean Region from crust to mantle. Springer, Berlin Heidelberg New York

Gentil L (1918) Notes d'un voyage géologique a Taza (Maroc septentrional) (Contribution a l'étude du Detroit Sudrifain). Bull Soc Geol Fr Ser 4(18):129–177

Hubbert MK (1937) Theory of scale models as applied to the study of geologic structures. Geol Soc Am Bull 48:1459–1520

Jabour H, Morabet Al M., Bouchta R (2000) Hydrocarbon systems of Morocco. In: Crasquin-Soleau S, Barrier E' (eds) Peri-Tethys Memoir 5: New data on Peri-Tethyan sedimentary basins. Mém Mus Natn Hist Nat 182:143–158

Jacobshagen VH, Gorler K, Giese P (1988) Geodynamic evolution of the Atlas system. In: Jacobshagen H (eds) The Atlas system of Morocco. Springer, Berlin Heidelberg New York, pp 481–499

Laville E, Piqué A (1991) La distension crustale atlantique et atlasique au Maroc au début du Mésozoïque: le rejeu des structures hercyniennes. Bull Soc Géol Fr 162:1161–1171

Laville E, Piqué A, Amrhar M, Charroud M (2004) A restatement of the Mesozoic Atlasic Rifting (Morocco). J Afr Earth Sci 38:145–153

Levy RG, Tilloy R (1952) Maroc Septentrional (Chaine du Rif), partie B. Livret-Guide des escursions A31 et C31. Congres Geologique International, XIX session. Alger 1952, série: Maroc 8:65

Michard A (1976) Elements de Géologie Marocaine. Notes Mém Serv Géol Maroc 252:408

Moratti G, Piccardi L, Vannucci G, Belardinew ME, Dahmani M, Bendkik A, Chenakeb M (2003) The 1755 ''Meknes'' Earthquake (Morocco): field data and geodynamic implications. J Geodyn 36:305–322

Morel JL (1988) Evolution recente de l'orogene rifain et de son avant pays depuis la fin de la mise en place des nappes (Rif-Maroc). Mem Geodiffusion 4:584

Morel JL (1989) Etats de contrainte et cinématique de la chaine rifaine (Maroc) du Tortonien à l'actuel. Geodinamica Acta 3:238–294

Morel JL, Zouine EM, Poisson A (1993) Relations entre la subsidence des bassins moulouyens et la création des relief atlasiques (Maroc): un example d'inversion tectonique depuis le Néogène. Bull Soc Geol Fr 164:79–91

Morley CK (1986) A classification of thrust fronts. Am Ass Pet Geol 70:12–25

Morley CK, Woganan N, Sankumarn N, Hoon TB, Alief A, Simmons M (2001) Late Oligocene—recent stress evolution in rift basins of northern and central Thailand: implications for escape tectonics. Tectonophysics 334:115–150

Morley CK, Back S, Rensbergen P, Crevello P, Lambiase JJ (2003) Characteristics of repeated, detached, Miocene–Pliocene tectonic inversion events, in a large delta province on an active margin, Brunei Darussalam, Borneo. J Struct Geol 25:1147–1169

Olsen PE (1997) Stratigraphic record of the early Mesozoic breakup of Pangea in the Laurasia–Gondwana rift system. Annu Rev Earth Planet Sci 25:337–401

Ramberg H (1981) Gravity, deformation and the Earth's crust in theory, experiments and geologic application, 2nd edn. Academic, London, pp 1–452

Suter G (1980a) Carte géologique de la Chaine Rifaine, échelle 1:500.000. Ministère de l'Energie et des Mines du Maroc, Direction de la Géologie, Rabat, Notes Mem Serv Geol Maroc 245a

Suter G (1980b) Carte structurale du Maroc, échelle 1:500.000. Ministère de l'Energie et des Mines du Maroc, Direction de la Géologie, Rabat. Notes Mem Serv Geol Maroc 245b

Taltasse P (1953) Recherches géologiques et hydrogéologiques dans le Bassin lacustre de Fès-Meknès. Notes Mem Serv Géol Maroc 115:1–300

Tilloy R (1955) Notice explicative de Feuille Fes-ouest de la Carte Geologique du maroc au 1:100.000. Notes Mem Serv Géol Maroc 109:1–62

Vannucchi P, Bettelli G (2002) Mechanics of subduction accretion as implied from the broken formations in the Apennines, Italy. Geology 30:835–838

Vially R, Letouzey J, Bénard F, Haddadi N, Desforges G, Asri H, Boudjema A (1994) Basin inversion along the North African Margin: The Saharan Atlas (Algeria). In: Roure F (ed) Peri-Tethyan Platform. Éditions Technip Paris, pp 79–118

Weijermars R, Schmeling H (1986) Scaling of Newtonian and non-Newtonian fluid dynamics without inertia for quantitative modelling of rock flow due to gravity (including the concept of rheological similarity). Phys Earth Planet Inter 43:316–330

Weijermars R, Jackson MPA, Vendeville B (1993) Rheological and tectonic modelling of salt provinces. Tectonophysics 217:143–174

Wernli R (1988) Micropaléontologie du Néogène post-nappes du Maroc septentrional et description systématique des foraminifères planctoniques. Notes Mem Serv Géol Maroc 331:1–270

Yovanovitch B (1922) La géologie du pétrole au Maroc. Bull Soc Géol Fr Ser 4(22):234–245

Zizi M (1996a) Triassic–Jurassic extensional systems and their Neogene reactivation in Northern Morocco (the Rides Prerifaines and Guercif basin), Ph.D. Thesis, Rice University, pp 1–230

Zizi M (1996b) Triassic–Jurassic extension and Alpine inversion in the northern Morocco. In: Ziegler PA, Horvath F (eds) Peri-Tethys Memoir 2: Structure and prospects of the Alpine basins and forelands. Mem Mus Natn Hist Nat 170:87–101

Zizi M (2002) Triassic-Jurassic extensional systems and their Neogene reactivation in Northern Morocco (the Rides Prerifaines and Guercif basin). Notes Mem Serv Géol Maroc 416:1–138

Zouhri M, Lamouroux C, Buret C (2001) La Mamora, charnière entre la Meseta et le Rif: son importance dans l'évolution géodynamique post-paléozoïque du Maroc. Geodinamica Acta 14:361–372